UCLA
UCLA Previously Published Works

Title

Stromal Cell-SLIT3/Cardiomyocyte-ROBO1 Axis Regulates Pressure Overload-Induced Cardiac Hypertrophy

Permalink

https://escholarship.org/uc/item/8cg5n585

Journal

Circulation Research, 134(7)

ISSN

0009-7330

Authors

Liu, Xiaoxiao

Li, Baolei

Wang, Shuyun

et al.

Publication Date

2024-03-29

DOI

10.1161/circresaha.122.321292

Copyright Information

Peer reviewed

Circulation Research

ORIGINAL RESEARCH

Stromal Cell-SLIT3/Cardiomyocyte-ROBO1 Axis Regulates Pressure Overload-Induced Cardiac Hypertrophy

Xiaoxiao Liu,* Baolei Li⬚,* Shuyun Wang, Erge Zhang, Megan Schultz⬚, Marlin Touma, Andre Monteiro Da Rocha, Sylvia M. Evans⬚, Anne Eichmann⬚, Todd Herron⬚, Ruizhen Chen, Dingding Xiong, Alexander Jaworski⬚, Stephen Weiss, Ming-Sing Si⬚

BACKGROUND: Recently shown to regulate cardiac development, the secreted axon guidance molecule SLIT3 maintains its expression in the postnatal heart. Despite its known expression in the cardiovascular system after birth, SLIT3's relevance to cardiovascular function in the postnatal state remains unknown. As such, the objectives of this study were to determine the postnatal myocardial sources of SLIT3 and to evaluate its functional role in regulating the cardiac response to pressure overload stress.

METHODS: We performed in vitro studies on cardiomyocytes and myocardial tissue samples from patients and performed in vivo investigation with SLIT3 and ROBO1 (roundabout homolog 1) mutant mice undergoing transverse aortic constriction to establish the role of SLIT3-ROBO1 in adverse cardiac remodeling.

RESULTS: We first found that *SLIT3* transcription was increased in myocardial tissue obtained from patients with congenital heart defects that caused ventricular pressure overload. Immunostaining of hearts from WT (wild-type) and reporter mice revealed that SLIT3 is secreted by cardiac stromal cells, namely fibroblasts and vascular mural cells, within the heart. Conditioned media from cardiac fibroblasts and vascular mural cells both stimulated cardiomyocyte hypertrophy in vitro, an effect that was partially inhibited by an anti-SLIT3 antibody. Also, the N-terminal, but not the C-terminal, fragment of SLIT3 and the forced overexpression of *SLIT3* stimulated cardiomyocyte hypertrophy and the transcription of hypertrophy-related genes. We next determined that ROBO1 was the most highly expressed roundabout receptor in cardiomyocytes and that ROBO1 mediated SLIT3's hypertrophic effects in vitro. In vivo, Tcf21+ fibroblast and Tbx18+ vascular mural cell-specific knockout of SLIT3 in mice resulted in decreased left ventricular hypertrophy and cardiac fibrosis after transverse aortic constriction. Furthermore, α-MHC+ cardiomyocyte-specific deletion of ROBO1 also preserved left ventricular function and abrogated hypertrophy, but not fibrosis, after transverse aortic constriction.

CONCLUSIONS: Collectively, these results indicate a novel role for the SLIT3-ROBO1–signaling axis in regulating postnatal cardiomyocyte hypertrophy induced by pressure overload.

GRAPHIC ABSTRACT: A graphic abstract is available for this article.

Key Words: axon guidance ■ fibroblasts ■ fibrosis ■ myocytes, cardiac ■ ROBO1 ■ stromal cells ■ ventricular pressure

---

Meet the First Author, see p 836

Chronic cardiac pressure overload is encountered in multiple conditions such as systemic arterial hypertension, congenital heart disease, ischemic heart disease, and pulmonary arterial hypertension.[1–5] A universal myocardial response to chronic pressure overload is hypertrophy, or the thickening of the ventricular walls,[6]

NOVELTY AND SIGNIFICANCE

What Is Known?

- SLIT3 is a secreted, axon guidance molecule that also regulates heart development.
- SLIT3 is also expressed in the postnatal heart, but its cardiovascular function remains unclear.

What New Information Does This Article Contribute?

- SLIT3 is produced by cardiac stromal cells, specifically cardiac fibroblasts, and vascular mural cells.
- SLIT3 stimulates cardiac hypertrophy and cardiac fibrosis under conditions of pressure overload.
- SLIT3 can stimulate cardiomyocyte hypertrophy via the ROBO1 receptor.

Prior work indicated the importance of the axon guidance molecule SLIT3 in cardiac development. The rationale for this study was to determine the postnatal role of SLIT3 in regulating adverse cardiac remodeling (cardiac hypertrophy and fibrosis) induced by pressure overload. We found that SLIT3, produced by cardiac stromal cells, that is, cardiac fibroblasts and vascular mural cells, can stimulate hypertrophy and fibrosis induced by pressure overload. We also found that SLIT3 can directly stimulate cardiomyocyte hypertrophy via the ROBO1 receptor. These findings indicate, for the first time, the role of SLIT3 in the postnatal heart in health and adverse cardiac remodeling. These results unveil a novel cardiac stromal cell-cardiomyocyte axis that may be targeted to reduce adverse cardiac remodeling.

Nonstandard Abbreviations and Acronyms

CNM	cardiac nonmyocyte
Fn	fibronectin
LV	left ventricle
NG2	neural/glial antigen 2
NRCM	neonatal rat cardiomyocyte
PDGFRA	platelet-derived growth factor receptor A
PDGFRB	platelet-derived growth factor receptor B
POSTN	periostin
TAC	transverse aortic constriction
WT	wild type

and fibrosis, or the increased deposition of extracellular matrix such as fibrillar collagen.[7] On a cellular level, cardiac hypertrophy derives from the addition of sarcomere units, leading to cardiomyocyte enlargement in the cross-sectional area.[6] While cardiac hypertrophy is a physiological response to exercise and pregnancy,[8–10] under chronic pressure overload conditions, this type of myocardial remodeling becomes pathological and is one of the most significant risk factors for the development of heart failure[6,11–14] and lethal ventricular arrhythmias.[15–17] Pathological cardiac hypertrophy precedes many forms of heart failure with systolic dysfunction, diastolic dysfunction, or a combination of both.[6,11,12] Cardiac fibrosis that develops in response to pressure overload also contributes to diastolic dysfunction.[7] Thus, preventing the development of adverse cardiac remodeling in the form of pathological cardiac hypertrophy and cardiac fibrosis would benefit many patients.[18–20] However, the continued high morbidity and mortality seen with heart failure,

a major public health concern that affects nearly 7 million patients in the United States[21] is indicative of ineffective therapies as well as an incomplete understanding of the mechanisms that drive adverse cardiac remodeling.

In both contexts of cardiac health and disease, accumulating evidence has indicated that cross-talk between cardiac nonmyocytes (CNMs) and cardiomyocytes plays a pivotal role in myocardial remodeling under various loading conditions.[22] Specifically, CNM-derived mediators may act in a paracrine fashion to stimulate cardiomyocyte hypertrophy and modulate their contractile function under increased afterload. Identification of these factors will provide insight into mechanisms of the cardiomyocyte hypertrophic response and may lead to the revelation of potential therapeutic targets for pathological cardiac hypertrophy.[23]

Recently, we observed that SLIT3, a large and secreted glycoprotein, is produced by fibrillar collagen-producing cells, and global and constitutive SLIT3 deficiency attenuated cardiac fibrosis under conditions of pressure overload.[24] We also found that SLIT3 stimulated adult cardiac fibroblasts to proliferate, produce collagen, and become contractile in vitro. Intriguingly, global and constitutive SLIT3 deficiency, throughout development and the postnatal state, was also associated with decreased hypertrophy, preserved ventricular systolic function, and improved survival of mice after the transverse aortic constriction (TAC).[24] These observations indicate that the developmental absence of SLIT3 modulates the hypertrophic response; however, the precise role played by SLIT3 in the adult heart remains unknown and is the focus of the current study.

SLIT3 belongs to the family of SLIT proteins, which was initially characterized as a repulsive guidance cue for neuronal axons.[25] Subsequently, the highly conserved SLIT ligands have been shown to participate in diverse

developmental processes and the regulation of several cellular functions.[26–29] Full-length SLIT ligands are cleaved by an unknown protease into N- and C-terminal fragments, which can bind to the ROBO receptors[26] and plexins,[30] respectively. *Slit3* is the predominant *Slit* transcribed in the embryonic mouse heart.[31] Nevertheless, it is unknown whether SLIT3 modulates cardiac hypertrophy indirectly, such as via modulation of the secretion of hypertrophic factors by fibroblasts, directly by binding to a cardiomyocyte cell-surface receptor, or as a result of a developmental defect resulting from constitutive SLIT3 deficiency that could lead to a defective hypertrophic response in the postnatal period.

To fill these knowledge gaps, we utilized inducible and conditional knockout mice in the current study to investigate the postnatal and tissue-specific roles of SLIT3 in regulating cardiac hypertrophy. Here, we show that cardiac fibroblast and vascular mural cell–mediated SLIT3 directly regulates the hypertrophic response of postnatal cardiomyocytes in response to pressure overload, and this stimulatory effect occurs via the ROBO1 receptor.

METHODS

Data Availability

The data that support the findings of this study are available from the corresponding author upon reasonable request. Please see the Supplemental Material for a detailed description.

RESULTS

Inducible Global-SLIT3 Deficiency Inhibits Pressure Overload–Induced Adverse Cardiac Remodeling and Ventricular Dysfunction

Consistent with our previous work in a TAC mouse model,[24] *Slit3* transcription in the adult wild-type (WT) mouse left ventricle (LV) was rapidly induced by pressure overload and reached its peak 2 weeks after TAC (Figure S1A), suggesting that the postnatal expression of this ligand may be induced by pressure overload.[24] To determine whether this finding would extend to humans, we queried our biorepository (the UCLA CHD-BioCore) to determine the level of *SLIT3* transcription in an RNA sequencing database of resected ventricular outflow tract tissue samples from patients with control (normal hearts declined for transplant) and pressure overload–causing congenital heart disease (subaortic membrane and tetralogy of Fallot). Significantly increased *SLIT3* transcript levels were observed in ventricular tissue from patients with pressure overload–induced hypertrophy (Figure 1A), supporting the contention that SLIT3 plays a role in postnatal cardiac hypertrophy under pressure overload. We also analyzed a potential association

between *SLIT3* expression and cardiac fibrosis in myocardial samples obtained from normal controls, patients with tetralogy of Fallot, where cardiac fibrosis is anticipated from the pressure overload,[32] and those with ventricular septal defect, where less cardiac fibrosis is anticipated from this volume overload defect.[33] We found that *SLIT3* transcript levels were significantly correlated with *COL1A1* transcript levels when considering all patient and control samples (Figure S1B). Furthermore, higher *SLIT3* and *COL1A1* transcript levels were found in myocardial samples taken from pressure overload defect patients (Figure S1B).

To directly interrogate the presence of a postnatal role of SLIT3 in the heart and its response to pressure overload, we generated tamoxifen-inducible SLIT3 global knockout mice (*Rosa26-CreERT2;Slit3^{fl/fl}*)[34,35] with the non-Cre-expressing littermates (*Slit3^{fl/fl}*) serving as controls. Immunofluorescence analysis confirmed a significant reduction of SLIT3 in hearts from *Rosa26-CreERT2;Slit3^{fl/fl}* mice at 6 weeks after tamoxifen induction compared with that in *Slit3^{fl/fl}* control mouse hearts (Figure 1B). Experimental and control mice were administered tamoxifen at 7 weeks of age and then, 2 weeks later, subjected to sham or TAC surgery, with the experiments terminated 4 weeks later (Figure 1C). Only TAC mice with a peak pressure gradient >35 mm Hg were included in downstream studies. The LV afterload in *Rosa26-CreERT2 Slit3^{fl/fl}* mice and *Slit3^{fl/fl}* control mice were not significantly different following TAC surgery (Figure S1C). We confirmed a significant and substantial reduction in *Slit3* transcript levels in *Rosa26-CreERT2;Slit3^{fl/fl}* mice (Figure 1D). After TAC, *Slit3^{fl/fl}* control mice experienced decreased ejection fraction and fractional shortening, along with increased end-diastolic LV posterior wall thickness and LV mass compared with control mice undergoing sham surgery (Figure 1E). By contrast, *Rosa26-CreERT2;Slit3^{fl/fl}* mice undergoing TAC manifested significantly improved ejection fraction and fractional shortening and reduced end-diastolic LV posterior wall thickness and LV mass after TAC surgery (Figure 1E).

In tandem with these stress-induced echocardiogram changes, *Slit3^{fl/fl}* mice undergoing TAC had more hypertrophy, manifested by a larger heart size, higher ratios of heart weight to body weight, and increased cardiomyocyte cross-sectional area compared with mice subjected to sham surgery (Figure 1F through 1H). Importantly, these hypertrophic changes induced by TAC were markedly attenuated in *Rosa26-CreERT2;Slit3^{fl/fl}* mice (Figure 1F through 1H). Moreover, transcript levels of several hypertrophy-related genes, including *Acta1*, *Nppa*, *Nppb*, and *Myh7*, were increased in *Slit3^{fl/fl}* control mice after TAC, while these increases were blunted by SLIT3 deletion in *Rosa26-CreERT2;Slit3^{fl/fl}* mice (Figure 1I).

Fibrosis-related gene expression was also examined in the LV tissue of explanted hearts from
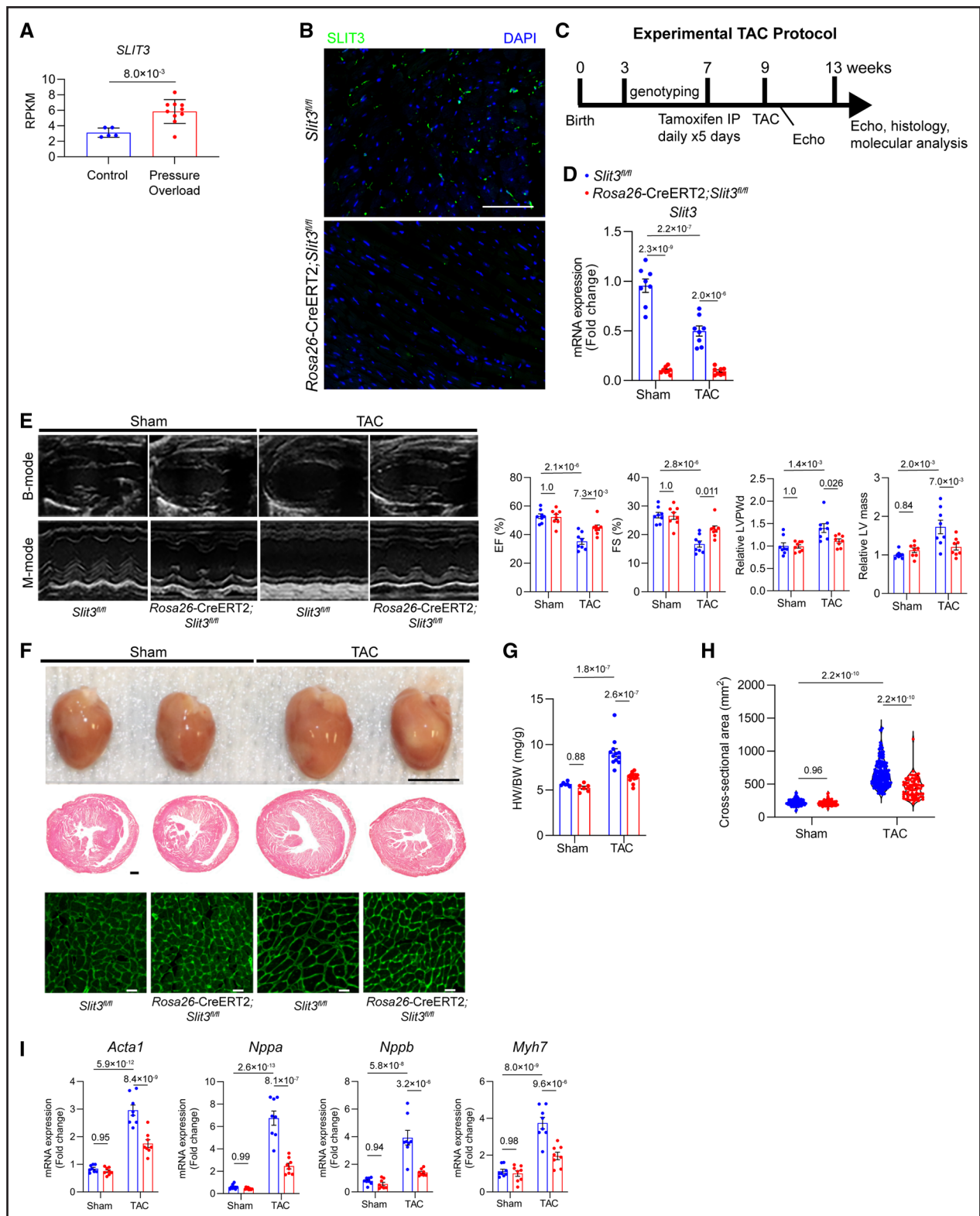
Figure 1. Inducible global-*SLIT3* deficiency alleviates the development of cardiac hypertrophy and dysfunction after transverse aortic constriction (TAC).

A, *SLIT3* transcription as measured by RNA sequencing and displayed as reads per kilobase of transcript per million mapped reads (RPKM) in ventricular tissue samples from normal controls and patients with pressure overload induced by congenital heart disease. Each data point represents a unique subject. Comparison performed with Mann-Whitney *U* test. **B**, Immunofluorescence staining of myocardial sections *Slit3^fl/fl^* and *Rosa26-CreERT2;Slit3^fl/fl^* mice 4 wk after tamoxifen injection using anti-SLIT3 antibody (green) and DAPI (blue) demonstrated loss of SLIT3 in the *Rosa26-CreERT2;Slit3^fl/fl^* mice. Scale bar, 500 µm. **C**, TAC experimental design and timeline. **D**, *Slit3* transcript levels in hearts from *Slit3^fl/fl^* and *Rosa26-CreERT2;Slit3^fl/fl^* mice after sham or TAC surgery. **E**, B-mode and M-mode echocardiography in *Slit3^fl/fl^* and (*Continued*)

Rosa26-CreERT2;Slit3^{fl/fl} mice and compared with those of control mice 4 weeks after sham or TAC surgery (Figure 2A). The transcript levels of *Col1a1* and *Col3a1* were markedly decreased in both sham and TAC groups of *Rosa26-CreERT2;Slit3^{fl/fl}* mice compared with *Slit3^{fl/fl}* control mice. *Acta2* transcription was not different between sham groups but significantly decreased in *Rosa26-CreERT2;Slit3^{fl/fl}* mice under pressure overload conditions. To visualize the accumulation of fibrillar collagen in the ventricular myocardium, we performed picrosirius red staining (Figure 2B). The quantity of fibrillar collagen in the hearts of *Rosa26-CreERT2;Slit3^{fl/fl}* mice was significantly less than in *Slit3^{fl/fl}* control mice as determined by the amount of red fluorescence intensity under polarized light (Figure 2B and 2C). Furthermore, we confirmed this result by biochemically measuring the amount of cardiac collagen using the hydroxyproline assay (Figure 2D). As the differentiation of resting resident cardiac fibroblasts to activated myofibroblasts is key to the development of cardiac fibrosis,[36,37] we further examined the expression of POSTN (periostin), a marker for myofibroblasts and fibroblast activation,[37–39] in post-TAC mouse heart tissue. We found that the transcript levels of *Postn* were increased in control mice after TAC and that acute, global Slit3 deficiency abrogated this inductive response (Figure 2E). This corresponded to decreased myocardial POSTN expression after TAC in SLIT3 deficient animals (Figure 2F through 2H). Taken altogether, these data indicate that SLIT3 has a postnatal role in regulating cardiac hypertrophy and fibrosis in response to pressure overload.

Fibroblast-Specific Deletion of SLIT3 Reduces Post-TAC Adverse Cardiac Remodeling and Ventricular Dysfunction

In light of the above findings and that SLIT3 is a secreted molecule, we hypothesized that the SLIT3 ligand serves a paracrine role in regulating cardiac hypertrophy and fibrosis. To define the cellular sources of cardiac SLIT3 in homeostatic and pressure overload conditions, we first separated cardiomyocytes from CNMs in isolated hearts of mice subjected to sham surgery or TAC. After confirming the purity of the isolated cell fractions (Figure 3A), we found that the CNM cell fraction exhibited several-fold higher levels of *Slit3* transcripts compared with the cardiomyocyte fraction from WT mouse hearts after TAC (Figure 3B).

As cardiac fibroblasts and vascular mural cells are myocardial stromal cells that comprise a large fraction of the CNMs of the heart,[40,41] we next evaluated the importance of each cell type as a myocardial SLIT3 source. Given that expression of *Tcf21* is a quiescent cardiac fibroblast marker,[42] we immunostained hearts recovered from *Tcf21-MerCreMer;Rosa26-tdTomato* reporter mice with an anti-SLIT3 antibody and confirmed SLIT3 expression associated with this cell population (Figure 3C), consistent with immunostaining of WT hearts (Figure S2A). The tdTomato+ cell population in these reporter mice also expressed PDGFRA (platelet-derived growth factor receptor A; Figure S2B). Next, we crossed *Slit3^{fl/fl}* mice with *Tcf21-MerCreMer* transgenic mice to obtain tamoxifen-inducible and fibroblast-specific SLIT3 knockout mice. After tamoxifen administration at 7 weeks (Figure 1C), we subjected *Tcf21-MerCreMer;Slit3^{fl/fl}* experimental and *Slit3^{fl/fl}* control mice to sham surgery or TAC. There was no difference in the TAC gradient of the 2 groups as determined by echocardiography (Figure S2C), and *Slit3* transcript levels were significantly decreased in experimental animals (Figure 3D), confirming Cre-mediated recombination. Under these conditions, echocardiograms performed 4 weeks after TAC demonstrated that ventricular hypertrophy (as measured by end-diastolic LV posterior wall thickness and LV mass) and LV dysfunction (as measured by ejection fraction and fractional shortening) were attenuated in cardiac fibroblast–targeted mice (Figure 3E). This finding was corroborated by a smaller heart, decreased heart weight to body weight ratio, and smaller cardiomyocyte cross-sectional area in Tcf21+ fibroblast-specific knockout of SLIT3 (Figure 3F through 3H) after TAC. In addition, *Slit3* deletion restricted in fibroblasts in *Tcf21-MerCreMer;Slit3^{fl/fl}* mice significantly reduced TAC-induced myocardial expression of hypertrophy-related and fibrosis-related genes compared with *Slit3^{fl/fl}* control mice (Figure 3I). Taken together, these studies demonstrated that SLIT3 produced in cardiac fibroblasts plays an important role in the hypertrophic response to pressure overload.

Moreover, *Tcf21-MerCreMer;Slit3^{fl/fl}* mice in both Sham and TAC groups also exhibited reduced cardiac

---

Figure 1 Continued. *Rosa26-CreERT2; Slit3^{fl/fl}* mice after sham or TAC surgery with analysis of ejection fraction (EF), shortening fraction (FS), relative left ventricle posterior wall thickness at diastole normalized to mice body weight (end-diastolic left ventricle posterior wall thickness [LVPWd]), relative left ventricle mass, and normalized to body weight. N=8 mice/group. **F**, Explanted hearts from *Slit3^{fl/fl}* and *Rosa26-CreERT2;Slit3^{fl/fl}* mice after sham or TAC surgery (**top**), representative images of heart sections stained with hematoxylin & eosin (H&E; scale bar, 500 μm; **middle**), and representative images of wheat germ agglutinin (WGA) staining of myocardial sections (scale bar, 20 μm, **bottom**). **G**, Heart weight to body weight (HW/BW) ratio in *Slit3^{fl/fl}* or *Rosa26-CreERT2;Slit3^{fl/fl}* mice after sham or TAC surgery. N=8 mice in each group. **H**, Quantification of myocyte cross-sectional area from WGA staining. N=400 cells from 6 to 8 mice in each group. **I**, Quantitative PCR (qPCR) analysis of transcript levels of hypertrophy-associated genes (*Nppa*, *Nppb*, *Myh7*, and *Acta1*, normalized to *Gapdh* transcript levels) in hearts from *Slit3^{fl/fl}* and *Rosa26-CreERT2;Slit3^{fl/fl}* mice after sham or TAC surgery. N=8 mice in each group. Two-way ANOVA with the Tukey multiple comparisons test used in (**D** through **I**). DAPI indicates 4′,6-diamidino-2-phenylindole.
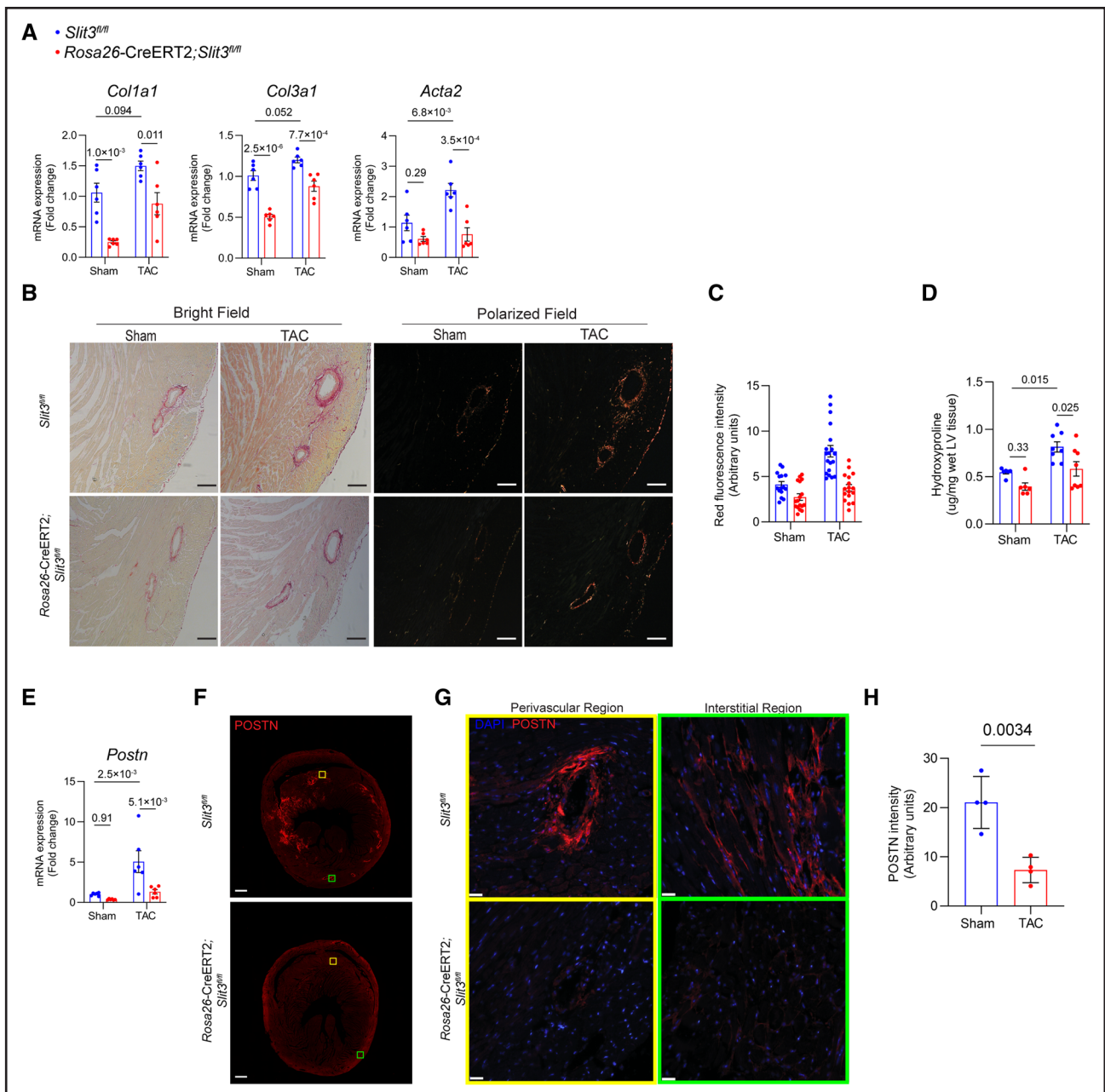
Figure 2. Inducible global-SLIT3 deficiency alleviates the development of cardiac fibrosis after transverse aortic constriction (TAC).

A, Quantitative PCR (qPCR) analysis of transcript levels of fibrosis-associated genes (*Col1a1*, *Col3a1*, and *Acta2*, normalized to *Gapdh* transcript levels) in hearts from *Slit3^fl/fl^* and *Rosa26-CreERT2;Slit3^fl/fl^* mice after sham or TAC surgery. N=8 mice in each group. **B**, Picrosirius red staining of myocardial sections from *Slit3^fl/fl^* and *Rosa26-CreERT2;Slit3^fl/fl^* mice after sham or TAC surgery and visualized under brightfield microscopy and polarized light. Representative images are shown. Scale bar, 100 μm. **C**, Quantification of red channel signal under polarized light of picrosirius red–stained myocardial sections from (**B**). Data from N=4 to 5 animals/group with 3 to 4 high power fields analyzed per animal. **D**, Collagen content determination from left ventricle tissue using the hydroxyproline assay. Data from n=8 animals/group. **E**, *Postn* transcript levels in hearts from *Slit3^fl/fl^* and *Rosa26-CreERT2;Slit3^fl/fl^* mice after sham or TAC surgery. Data from N=8 animals/group. **F** and **G**, Representative images of post-TAC myocardial sections stained with an anti-POSTN (periostin) antibody (scale bar=100 μm in [**F**] and 25 μm in [**G**]). **H**, Quantification of POSTN stained myocardial sections in (**F**). N=4 mice in each group. Two-way ANOVA with the Tukey multiple comparisons test used in (**A**, **D**, and **E**). A linear regression model with cluster option was used to evaluate the data in (**C**), where the comparison of genotype (*Slit3^fl/fl^* vs *Rosa26-CreERT2;Slit3^fl/fl^*) and surgery (sham vs TAC) and the interaction between genotype and surgery were all found to be significant ($P < 1.0 \times 10^{-4}$ for all comparisons and interaction). Two-tailed *t* test was used in (**H**), with data passing the Shapiro-Wilk normality test and assuming the application of the central limit theorem.
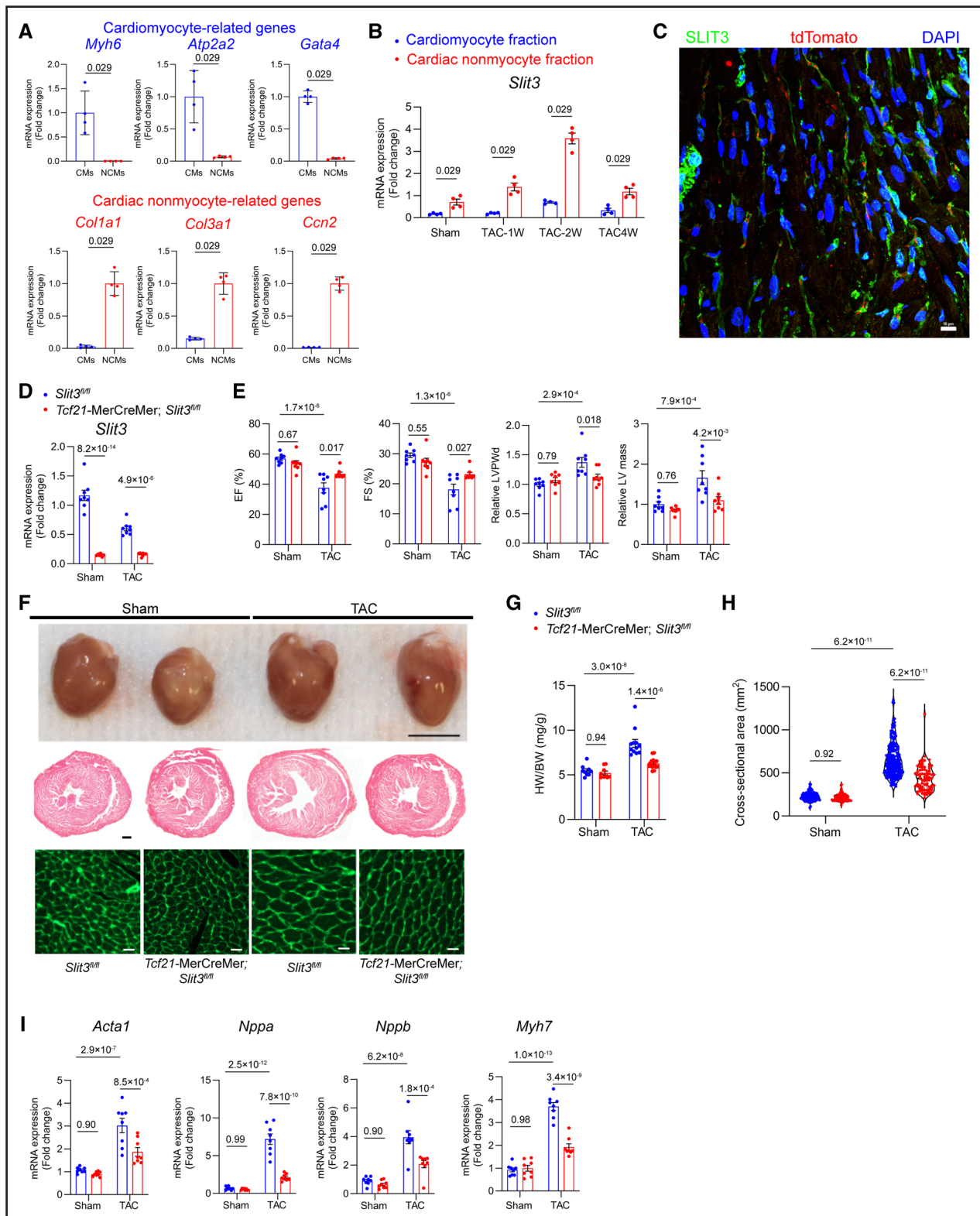
Figure 3. Fibroblast-specific deletion of SLIT3 reduces cardiac hypertrophy and dysfunction after transverse aortic constriction (TAC).

A, Isolation of cardiac nonmyocyte (NCM) and cardiomyocyte (CM) cellular fractions from adult wild-type (WT) mice was verified by measuring *Col1a1*, *Col3a1*, *Ccn2*, *Myh7*, *Myh6*, and *Acta*1 mRNA levels (normalized to *Gapdh* transcript levels). Cells from N=4 WT mice and comparisons made with the Mann-Whitney *U* test. **B**, *Slit3* transcript levels in isolated NCM and CM fractions from adult mouse hearts subjected to sham or TAC surgery. N=4 mice/group and comparisons were made with the Mann-Whitney *U* test. **C**, Immunofluorescence staining of a heart section from *Tcf21-CreERT2;Rosa26-tdTomato* mice using anti-SLIT3 antibody (green), anti-tdTomato (red), and 4',6-diamidino-2-phenylindole (DAPI; blue). Scale bar, 50 μm. **D**, *Slit3* transcript levels determined by quantitative PCR (qPCR) in *Slit3^{fl/fl}* and *Tcf21-CreERT2;Slit3^{fl/fl}* mice (*Continued*)

fibrosis. Transcription of fibrillar collagen genes *Col1a1* and *Col3a1* were decreased in *Tcf21-MerCreMer; Slit3*^{fl/fl} mice that had undergone TAC (Figure 4A). Collagen content as determined by picrosirius red staining and polarized microscopy (Figure 4B and 4C) and LV hydroxyproline content (Figure 4D) was decreased in *Tcf21-MerCreMer;Slit3*^{fl/fl} mice after TAC. *Postn* transcript levels were decreased in *Tcf21-MerCreMer;Slit3*^{fl/fl} mice after TAC (Figure 4E). The amount of POSTN in the LV of *Tcf21-MerCreMer;Slit3*^{fl/fl} mice as determined by immunofluorescence was decreased compared with *Slit3*^{fl/fl} control mice after TAC (Figure 4F through 4H). These results indicate that cardiac fibroblast-mediated SLIT3 is important for the development of cardiac hypertrophy and fibrosis induced by pressure overload.

Vascular Mural Cell–Specific Deletion of SLIT3 Reduces Cardiac Hypertrophy and Dysfunction After TAC

In our previous work, immunofluorescence staining demonstrated that SLIT3 was localized not only to the cardiac interstitium but also to the mural cells of myocardial blood vessels.[24] Furthermore, we previously determined that human mesenchymal stem/stromal cells, which also reside in the perivascular region,[43] expressed SLIT3.[44] As such, we considered the possibility that SLIT3 derived from vascular mural cells in the heart may also play a role in regulating cardiac hypertrophy. To specifically target vascular mural cells, we utilized a *Tbx18-CreERT2* mouse that has been previously generated and characterized extensively to be a vascular mural cell–specific Cre mouse line with minimal crossover into fibroblasts, endothelial cells, and cardiomyocytes.[45] Using *Tbx18-CreERT2;Rosa26-tdTomato* reporter mice, we confirmed that the tdTomato+ cells were located in the periendothelial region of myocardial vessels. Furthermore, these tdTomato+ vascular mural cells also expressed SLIT3 (Figure 5A) and PDGFRB (platelet-derived growth factor receptor B and vascular smooth muscle cell marker[46]), NG2 (neural/glial antigen 2 and pericyte marker[47]), and *MYH11* (vascular smooth muscle cell marker) by immunostaining[48] (Figure S3A through 3C). We also confirmed that *Tcf21-MerCreMer* and *Tbx18-CreERT2* reporter mice had different tdTomato expression patterns, with the *Tbx18-CreERT2* mice having predominantly a vascular

mural expression (Figure 5A; Figure 3A through S3C), while the *Tcf21-MerCreMer* had a more interstitial (Figure 3C; Figure S2B) and valvar staining pattern (Figure 4A).

Next, we crossed *Slit3*^{fl/fl} mice with *Tbx18-CreERT2* mice to obtain *Tbx18-CreERT2, Slit3*^{fl/fl} mice and their non-Cre expressing (*Slit3*^{fl/fl}) littermates. As described above, mice were then administered vehicle or tamoxifen and then subjected to sham surgery or TAC (Figure 1C). For the TAC groups, only mice with adequate arch gradients as determined by echocardiogram were chosen for further study (Figure S4B). Having confirmed that *Slit3* transcript levels were decreased in tamoxifen-treated *Tbx18-CreERT2;Slit3*^{fl/fl} mice (Figure 5B), echocardiography at 4 weeks after sham surgery or TAC revealed improved cardiac function and reduced LV wall thickness and mass in mural cell-targeted mice after TAC (Figure 5C). Grossly, hearts from the non–Cre-containing animals that had undergone TAC were larger and had a larger heart weight to body weight ratio than those from *Tbx18-CreERT2;Slit3*^{fl/fl} post-TAC mice (Figure 5D and 5E). Cardiomyocyte cross-sectional area was decreased in *Tbx18-CreERT2;Slit3*^{fl/fl} post-TAC mice, also consistent with decreased hypertrophy (Figure 5D and 5F), as well as attenuated TAC-stimulated transcription of *Acta1*, *Nppa*, *Nppb*, and *Myh7* (Figure 5G). Collectively, these results confirm that in addition to fibroblast-derived SLIT3, vascular mural cells also serve as a source of this ligand in regulating pressure overload–induced cardiac hypertrophy.

We also found that vascular mural cell–mediated SLIT3 affected the development of cardiac fibrosis induced by pressure overload. While the transcript levels of *Col3a1 and Acta2* were not significantly different between control and *Tbx18-CreERT2;Slit3*^{fl/fl} mice (Figure 6A), *Col1a1* transcript levels were decreased in *Tbx18-CreERT2;Slit3*^{fl/fl} mice compared with control mice after sham and TAC surgery (Figure 6A). Consistent with the changes in *Col1a1* transcript levels, fibrillar collagen content in *Tbx18-CreERT2;Slit3*^{fl/fl} hearts was markedly less as determined by picrosirius red staining followed by polarized light microscopy (Figure 6B and 6C) and the hydroxyproline assay of LV tissue from *Tbx18-CreERT2;Slit3*^{fl/fl} mice in both sham and TAC groups (Figure 6D). The *Postn* transcript and POSTN protein levels in the LVs after TAC were also decreased

---

Figure 3 Continued. after 13 wk after sham or TAC surgery. N=8 mice/group. **E**, Echocardiography data from *Slit3*^{fl/fl} and *Tcf21-CreERT2;Slit3*^{fl/fl} mice after sham or TAC surgery with analysis of ejection fraction, fractional shortening, relative end-diastolic left ventricle posterior wall thickness (LVPWd), and relative left ventricle mass. N=8 mice/group. **F**, Explanted hearts from *Slit3*^{fl/fl} control or *Tcf21-CreERT2;Slit3*^{fl/fl} mice after sham or TAC surgery (**top**); representative images of heart sections stained with hematoxylin & eosin (H&E; scale bar, 500 μm; **middle**); and representative images of wheat germ agglutinin (WGA) stained heart sections (scale bar, 20 μm; **bottom**). **G**, Heart weight to body weight (HW/BW) ratio. N=8 mice/group. **H**, Quantification of CM cross-sectional area from WGA-stained sections. N=400 cells from 6 to 7 mice in each group. **I**, qPCR analysis hypertrophy-related genes (*Nppa*, *Nppb*, *Myh7*, and *Acta1*, normalized to *Gapdh* mRNA levels) in hearts from *Slit3*^{fl/fl} and *Tcf21-CreERT2;Slit3*^{fl/fl} mice after sham or TAC surgery. N=8 mice/group. Two-way ANOVA with the Tukey multiple comparisons test used in (**D**, **E**, and **G–I**).
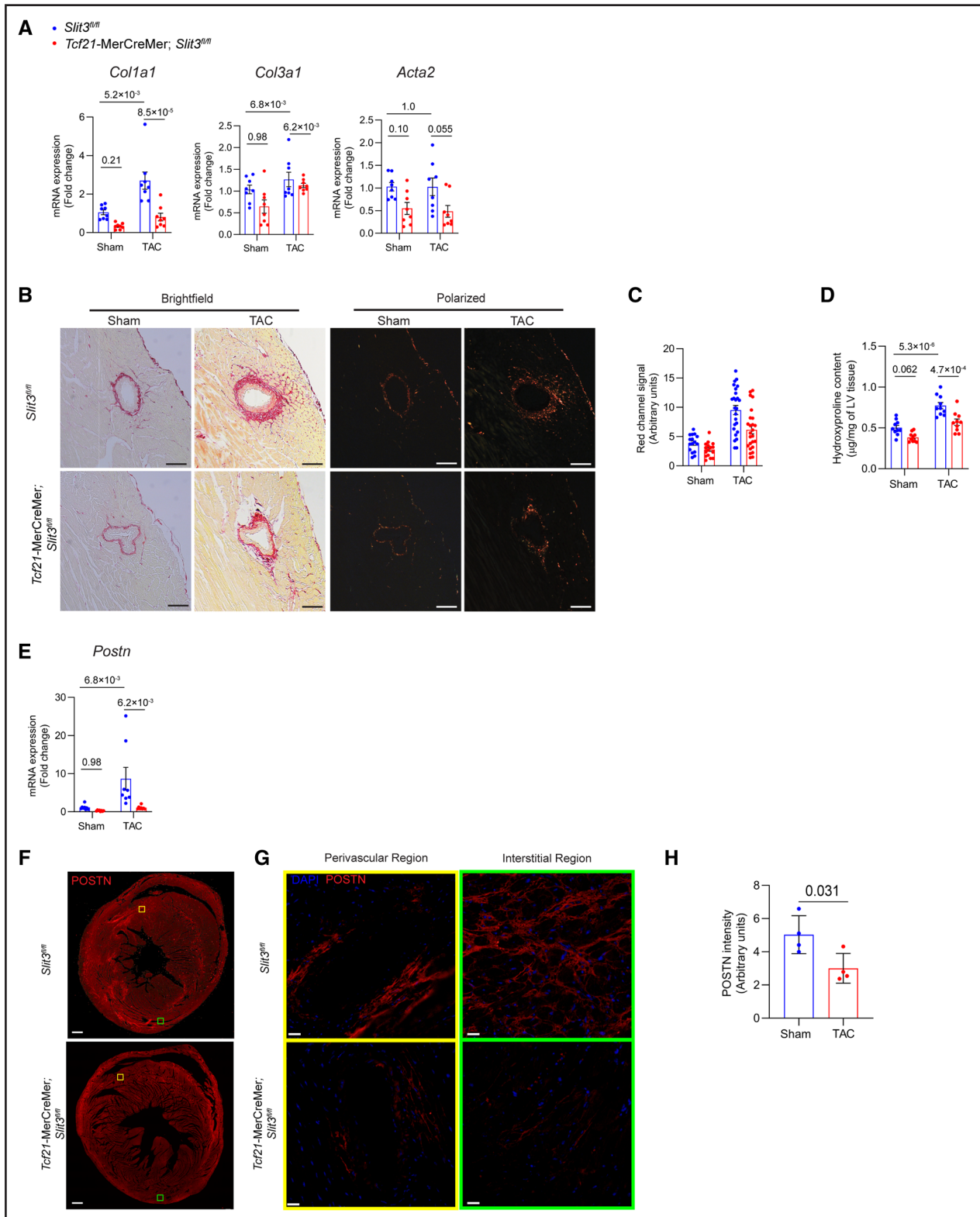
Figure 4. Fibroblast-specific deletion of *SLIT3* abrogates pressure overload–induced cardiac fibrosis.
A, Quantitative PCR (qPCR) analysis of transcript levels of fibrosis-associated genes (*Col1a1*, *Col3a1*, and *Acta2*, normalized to *Gapdh* transcript levels) in hearts from *Slit3*^fl/fl and *Tcf21*-MerCreMer;*Slit3*^fl/fl mice after sham or transverse aortic constriction (TAC) surgery. N=8 mice in each group. **B**, Picrosirius red staining of myocardial sections from *Slit3*^fl/fl and *Tcf21*-MerCreMer;*Slit3*^fl/fl mice after sham or TAC surgery and visualized under brightfield microscopy and polarized light. Representative images are shown. Scale bar, 100 µm. **C**, Quantification of red channel signal under polarized light of picrosirius red–stained myocardial sections from (**B**). Data from N=4 to 5 animals/group with 4 high power fields analyzed per animal. **D**, Collagen content determination from left ventricle tissue using the hydroxyproline assay. Data from n=8 (*Continued*)

in *Tbx18-CreERT2;Slit3^fl/fl* mice, indicating that loss of SLIT3 in vascular mural cells inhibited the activation of cardiac fibroblasts induced by pressure overload (Figure 6E through 6H).

Our in vivo studies demonstrated that global, fibroblast-specific, and vascular mural cell−specific deletion of SLIT3 appeared to decrease TAC-induced hypertrophy to the same degree (Figures 1, 3, and 5). However, we observed subtle differences in cardiac fibrosis in these different groups of mutant mice. Acute, global deletion of SLIT3 in *Rosa26-CreERT2;Slit3^fl/fl* mice resulted in the greatest decrease in *Col1a1*, *Col3a1*, and *Acta2* transcription in sham and TAC animals (Figure 2A). However, fibroblast-specific deletion of SLIT3 in *Tcf21-MerCreMer;Slit3^fl/fl* mice resulted in a significant decrease in *Col1a1* and *Col3a1* transcription only after TAC, but not sham, surgery (Figure 4A). Vascular mural cell−specific deletion of SLIT3 in *Tbx18-CreERT2;Slit3^fl/fl* mice appeared to have the least impact and resulted only in a decrease in *Col1a1* transcription after TAC surgery (Figure 6A). This differential impact on cardiac fibrosis genes paralleled the amount of reduction in LV *Slit3* transcripts in *Rosa26-CreERT2;Slit3^fl/fl* (Figure 1D), *Tcf21-MerCreMer;Slit3^fl/fl* (Figure 3D), and *Tbx18-CreERT2;Slit3^fl/fl* mice (Figure 5B). Thus, our in vivo results suggest that the adverse cardiac remodeling response to pressure overload is sensitive to the amount and source of SLIT3.

Fibroblast and Vascular Mural Cell−Derived SLIT3 Can Directly Induce Hypertrophy in Cardiomyocytes In Vitro

To further evaluate the ability of CNM-derived SLIT3 to directly trigger hypertrophic responses of cardiomyocytes, we conducted in vitro experiments by exposing neonatal rat cardiomyocytes (NRCMs) to conditioned media from cardiac fibroblasts and vascular mural cells isolated from SLIT3 global knockout or *Slit3^fl/fl* adult mice in vitro. Relative to conditioned media from WT (*Slit3^+/+*) adult mouse cardiac fibroblasts that stimulated cardiomyocyte hypertrophy, conditioned media from *Slit3* knockout (*Slit3^−/−*) cardiac fibroblasts did not stimulate hypertrophy or *Nppa* and *Nppb* transcription (Figure S5A through S5C). Likewise, when *Slit3^fl/fl* cardiac fibroblasts were transduced with a Cre-recombinase adenoviral vector (*AdCre*), *Slit3* expression was abolished (Figure S5D), and the conditioned media no longer induced a hypertrophic response

relative to cells transduced with a control GFP adenoviral vector (*AdGFP*; Figure S5E and S5F). By contrast, when *Slit3^fl/fl* cardiac fibroblasts were transduced with a *SLIT3*-expressing adenoviral construct (*AdSLIT3*), *Slit3* expression levels were increased and conditioned media from these cells increased NRCM size relative to controls in tandem with higher transcript level of *Nppa* and *Nppb* (Figure S5E through S5G). Furthermore, the addition of an anti-SLIT3 antibody inhibited the prohypertrophic effect of conditioned media from SLIT3 overexpressing adult mouse cardiac fibroblasts on NRCMs, as reflected in the downregulated expression of *Nppa* and *Nppb*, as well as smaller cell size compared with an isotype control IgG (Figure S5H through S5J). Furthermore, similar effects were observed using mural cell populations engineered to silence or increase *SLIT3* expression (Figure 6A through 6F).

These in vitro data suggested that fibroblast and vascular mural cell−mediated SLIT3 can stimulate cardiomyocyte hypertrophy. As SLITs can be cleaved into N- and C-terminal fragments in vivo,[49] we next investigated which portion of SLIT3 was responsible for stimulating cardiomyocyte hypertrophy because these fragments have been determined to bind to different receptors.[26,30] We cultured NRCMs with recombinant N- and C-terminal fragments of SLIT3 (SLIT3-NT and SLIT3-CT, respectively) and observed that only SLIT3-NT could promote the transcription of *Nppa* and *Nppb* and stimulate NRCMs hypertrophy (Figure S5K through S5M). Of note, SLIT3-NT also stimulated hypertrophic responses of human-induced pluripotent stem cell−derived cardiomyocytes (Figure S5N through S5P). Finally, forced expression of SLIT3 in NRCMs strongly induced hypertrophy (Figure S5G and S5H). Taken together, these results indicate that *SLIT3*, normally expressed by fibroblasts and vascular mural cells in the heart, can stimulate hypertrophy in cardiomyocytes.

The In Vitro Hypertrophic Effects of SLIT3 on Cardiomyocytes Are ROBO1-Dependent

The N-terminal fragment of SLIT proteins mediates their functions by binding to cognate transmembrane receptors belonging to the roundabout receptor family.[26] There are 4 mammalian ROBOs (ROBO1-4), each containing 5 immunoglobulin-like domains and FN (fibronectin) III motifs in the extracellular domain with the exception of ROBO4, which has only 2 immunoglobulin domains and

---

Figure 4 Continued. animals/group. **E**, *Postn* transcript levels in hearts from *Slit3^fl/fl* and *Tcf21-MerCreMer;Slit3^fl/fl* mice after sham or TAC surgery. Data from N=8 animals/group. **F** and **G**, Representative images of post-TAC myocardial sections stained with an anti-POSTN (periostin) antibody (scale bar=500 μm in [**F**] and 25 μm in [**G**]). **H**, Quantification of POSTN stained myocardial sections in (**F**). N=4 mice in each group. Two-way ANOVA with the Tukey multiple comparisons test used in (**A**, **D**, and **E**). A linear regression model with cluster option was used to evaluate the data in (**C**), where the comparison of genotype (*Slit3^fl/fl* vs *Tcf21-MerCreMer;Slit3^fl/fl*) and surgery (sham vs TAC) and the interaction between genotype and surgery were all found to be significant ($P=2.4\times10^{-3}$, $P<1.0\times10^{-4}$, and $P=6.5\times10^{-3}$, respectively). Two-tailed *t* test was used in (**H**), with data passing the Shapiro-Wilk normality test and assuming the application of the central limit theorem.
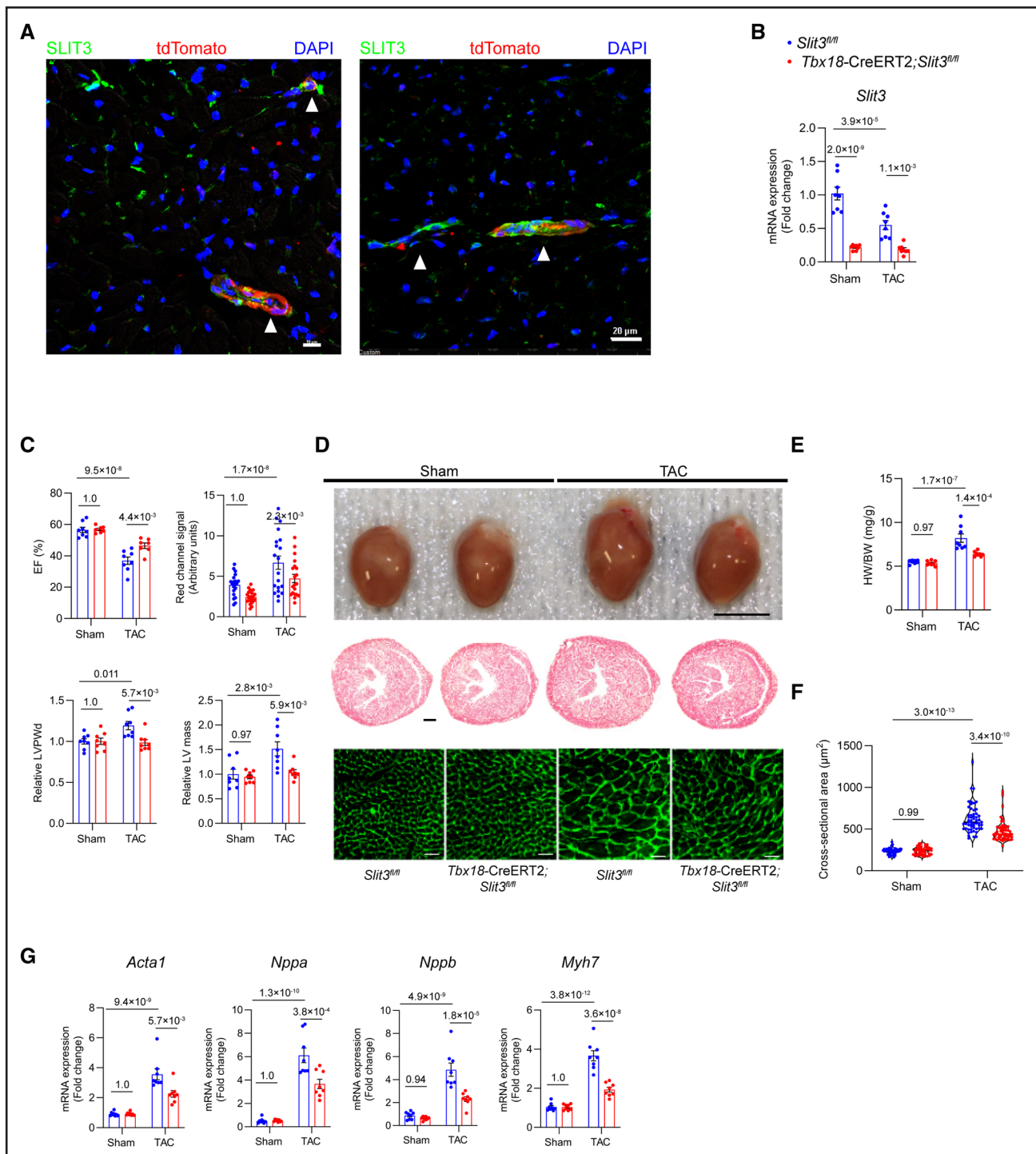
Figure 5. Vascular mural cell–specific deletion of SLIT3 reduces cardiac hypertrophy and dysfunction after transverse aortic constriction (TAC).

A, Immunofluorescence staining of heart sections from *Tbx18-CreERT2;Rosa26-Tdtomato* mice using anti-SLIT3 antibody (green), anti-tdTomato antibody (red), and 4',6-diamidino-2-phenylindole (DAPI; blue). White arrowheads denote the overlap of SLIT3 and *tdTomato* signals in the mural region of myocardial blood vessels in cross-section (**left**) and axially (**right**). Scale bar for (**left**), 10 μm. Scale bar for (**right**), 20 μm. **B**, *Slit3* transcription determined by quantitative PCR (qPCR; normalized to *Gapdh* transcript levels) in *Slit3$^{fl/fl}$* or *Tbx18-CreERT2;Slit3$^{fl/fl}$* mice hearts after sham or TAC surgery. N=8 mice/group. **C**, Echocardiographic studies of *Slit3$^{fl/fl}$* and *Tbx18-CreERT2;Slit3$^{fl/fl}$* mice after sham or TAC surgery. N=8 mice/group. **D**, Appearance of hearts explanted from *Slit3$^{fl/fl}$* control and *Tbx18-CreERT2;Slit3$^{fl/fl}$* mice after sham or TAC surgery (**top**); representative images of heart sections stained with hematoxylin & eosin (H&E; scale bar, 500 μm; **middle**); and representative images of heart sections stained with wheat germ agglutinin (WGA; scale bar, 20 μm; **bottom**). **E**, Heart weight to body weight (HW/BW) ratio. N=8 mice/group. **F**, Quantification of cardiomyocyte cross-sectional area on WGA staining. N=600 cells from 6 mice in each group. **G**, qPCR analysis of hypertrophy-associated gene transcription (*Nppa*, *Nppb*, *Myh7*, and *Acta1*, normalized to *Gapdh* mRNA expression) in hearts from *Slit3$^{fl/fl}$* control or *Tbx18-CreERT2, Slit3$^{fl/fl}$* mice after sham or TAC surgery. N=8 mice/group. Two-way ANOVA with the Tukey multiple comparisons test was used in all analyses. EF indicates ejection fraction; LV, left ventricle; and LVPWd, end-diastolic left ventricle posterior wall thickness.
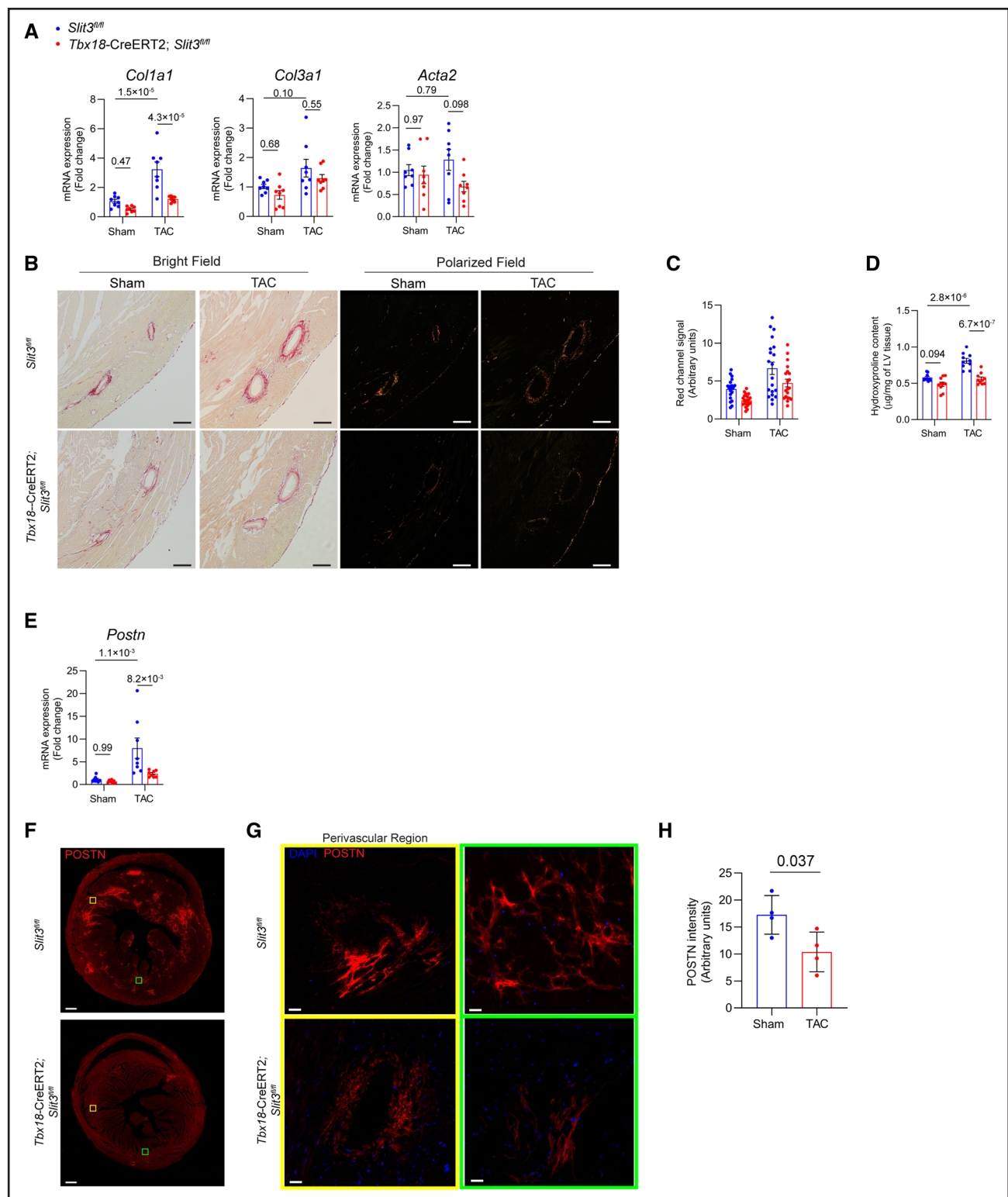
Figure 6. Vascular mural cell–specific deletion of SLIT3 abrogates pressure overload–induced cardiac fibrosis.
A, Quantitative PCR (qPCR) analysis of transcript levels of fibrosis-associated genes (*Col1a1*, *Col3a1*, and *Acta2*, normalized to *Gapdh* transcript levels) in hearts from *Slit3$^{fl/fl}$* and *Tbx18-CreERT2;Slit3$^{fl/fl}$* mice after sham or transverse aortic constriction (TAC) surgery. N=8 mice in each group.
B, Picrosirius red staining of myocardial sections from *Slit3$^{fl/fl}$* and *Tbx18-CreERT2;Slit3$^{fl/fl}$* mice after sham or TAC surgery and visualized under brightfield microscopy and polarized light. Representative images are shown. Scale bar, 100 µm. **C**, Quantification of red channel signal under polarized light of picrosirius red–stained myocardial sections from (**B**). Data from N=4 animals/group with 4 high power fields analyzed per animal.
D, Collagen content determination from left ventricle tissue using the hydroxyproline assay. Data from n=8 animals/group. **E**, *Postn* transcript levels in hearts from *Slit3$^{fl/fl}$* and *Tbx18-CreERT2;Slit3$^{fl/fl}$* mice after sham or TAC surgery. Data from N=8 animals/group. **F** and **G**, Representative images of post-TAC myocardial sections stained with an anti-POSTN (periostin) antibody (scale bar=500 µm in [**F**] and 25 µm in [**G**]). (*Continued*)

the Fn III motifs.[50] To determine the identity of the ROBO receptor that mediates SLIT3 effects on cardiomyocytes, we first measured the transcript levels of *Robo1*, *Robo2*, *Robo3*, and *Robo4* in adult mouse cardiomyocytes, NRCMs, and human-induced pluripotent stem cell–derived cardiomyocytes. We found that *Robo1* transcript levels were dominant in each of the cardiomyocyte populations (Figure 7A). Furthermore, TAC surgery stimulated *Robo1* transcription in the heart up to 4 weeks after TAC (Figure 7B). Interestingly, ROBO1 global knockout mice (*Robo1*$^{-/-}$) exhibited smaller cardiomyocytes compared with their WT control mice (*Robo1*$^{+/+}$) at the age of 7 days, phenocopying our observations in comparatively aged *Slit3* knockout mice (Figure 7C and 7D). Taken together, these findings suggested ROBO1 as a possible receptor on cardiomyocytes for SLIT3.

Previous reports demonstrated that a ROBO1-Fc fusion protein lacking its FN motifs can bind SLIT family member proteins in a soluble receptor ligand pull-down assay.[51,52] Hence, we examined the impact of ROBO1-Fc on the ability of conditioned media from SLIT3 overexpressing adult mouse cardiac fibroblasts to stimulate NRCM hypertrophy in vitro. Under these conditions, ROBO1-Fc inhibited the hypertrophic effects of the conditioned media from SLIT3 overexpressing adult mouse cardiac fibroblasts relative to isotype IgG controls (Figure S7). Next, NRCMs were transfected with *siScramble* or siRNA specifically targeting *Robo1* (si*Robo1*) before *AdGFP* or *AdSLIT3* transduction. Inhibition of *Robo1* transcription by si*Robo1* abrogated the hypertrophic effects of *AdSLIT3* on NRCMs (Figure 7E and 7F). We confirmed that these findings in SLIT3-NT stimulated human-induced pluripotent stem cell–derived cardiomyocytes where *siROBO1* also decreased the transcription of *NPPA* and *NPPB* (Figure 7G). Likewise, *siROBO1* inhibited baseline levels of *NPPA* and *NPPB* in iPSC-CMs as these cells can also express *SLIT3* (data not shown), which, thus, may act in an autocrine effect.

ROBO1 Regulates the Development of Pathological Cardiac Hypertrophy After TAC In Vivo

To directly investigate the function of ROBO1 in vivo, we generated *Robo1*$^{fl/fl}$ mice, in which the exon3 of the *Robo1* gene was flanked by *Loxp* (Figure 8A). Then, inducible and cardiomyocyte-specific knockout of *Robo1* mice was generated by crossing *Robo1*$^{fl/fl}$ mice with *Myh6-MerCreMer* mice. After tamoxifen administration, the knockout efficiency of ROBO1 in cardiomyocytes

was confirmed by immunofluorescence staining of heart tissue. ROBO1 expression was predominant on the cell membrane of cardiomyocytes in *Robo1*$^{fl/fl}$ control mice, and this signal was significantly abrogated in heart tissue from the *Myh6-MerCreMer;Robo1*$^{fl/fl}$ mice (Figure 8B). We also confirmed by quantitative PCR (qPCR) that *Robo1* transcription was effectively reduced in cardiomyocytes from *Myh6-MerCreMer;Robo1*$^{fl/fl}$ mice (Figure S8A). Sham or TAC surgery was conducted (Figure 1C), and only mice with an adequate TAC gradient were included in the downstream studies (Figure S8B). *Robo1* transcript levels were significantly decreased in hearts from *Myh6-MerCreMer;Robo1*$^{fl/fl}$ mice 1 month after TAC (Figure S8C). Mice with cardiomyocyte-specific deletion of *ROBO1* exhibited on echocardiogram improved cardiac function and reduced LV wall thickness and mass after TAC (Figure 8C), as well as a smaller heart weight to body weight ratio, heart size, and cross-sectional area after TAC compared with hearts from *Robo1*$^{fl/fl}$ littermate controls (Figure 8D through 8F). This was accompanied by downregulation of cardiac hypertrophy–associated genes such as *Nppa*, *Nppb*, *Myh7*, and *Acta1* (Figure 8G). Finally, cardiomyocyte-specific deletion of ROBO1 had no significant impact on pressure overload–induced cardiac fibrosis (Figure S8D and S8E). Taken together, these results indicate that SLIT3-ROBO1 regulates cardiac hypertrophy and dysfunction induced by pressure overload (Figure S9).

DISCUSSION

While *SLIT3* is known to partake in the embryonic development of the heart and other organs and is expressed in the adult state, the function of *SLIT3* in the postnatal cardiovascular system has up to now remained unknown. Our previous study demonstrated that *SLIT3* global knockout mice manifested a blunted fibrotic and hypertrophic response to pressure overload,[24] a phenotype that could have been the result of faulty developmental processes. In the present study, we provide several lines of evidence in humans and mice to demonstrate *SLIT3*'s essential role in regulating the hypertrophic and fibrotic response of the adult myocardium. To exclude the effects of *SLIT3* deficiency on cardiovascular development in our postnatal studies, we generated inducible and stromal cell–specific *SLIT3* knockout mice. Conditional and inducible deletion of *SLIT3* in fibroblasts or vascular mural cells alleviated the development of cardiac hypertrophy, fibrosis, and dysfunction after TAC, phenocopying the response in *SLIT3* global knockout

---

Figure 6 Continued. H, Quantification of POSTN stained myocardial sections in (**F**). N=4 mice in each group. Two-way ANOVA with the Tukey multiple comparisons test used in (**A**, **D**, and **E**). A linear regression model with cluster option was used to evaluate the data in (**C**), where the comparison of genotype (*Slit3*$^{fl/fl}$ vs *Tbx18*-CreER2;*Slit3*$^{fl/fl}$) and surgery (sham vs TAC) were different (*P*<1.0×10^{-4} and *P*<1.0×10^{-4}, respectively). The interaction between genotype and surgery was not significant (*P*=0.53). Two-tailed *t* test used in (**H**), with data passing the Shapiro-Wilk normality test and assuming the application of the central limit theorem.
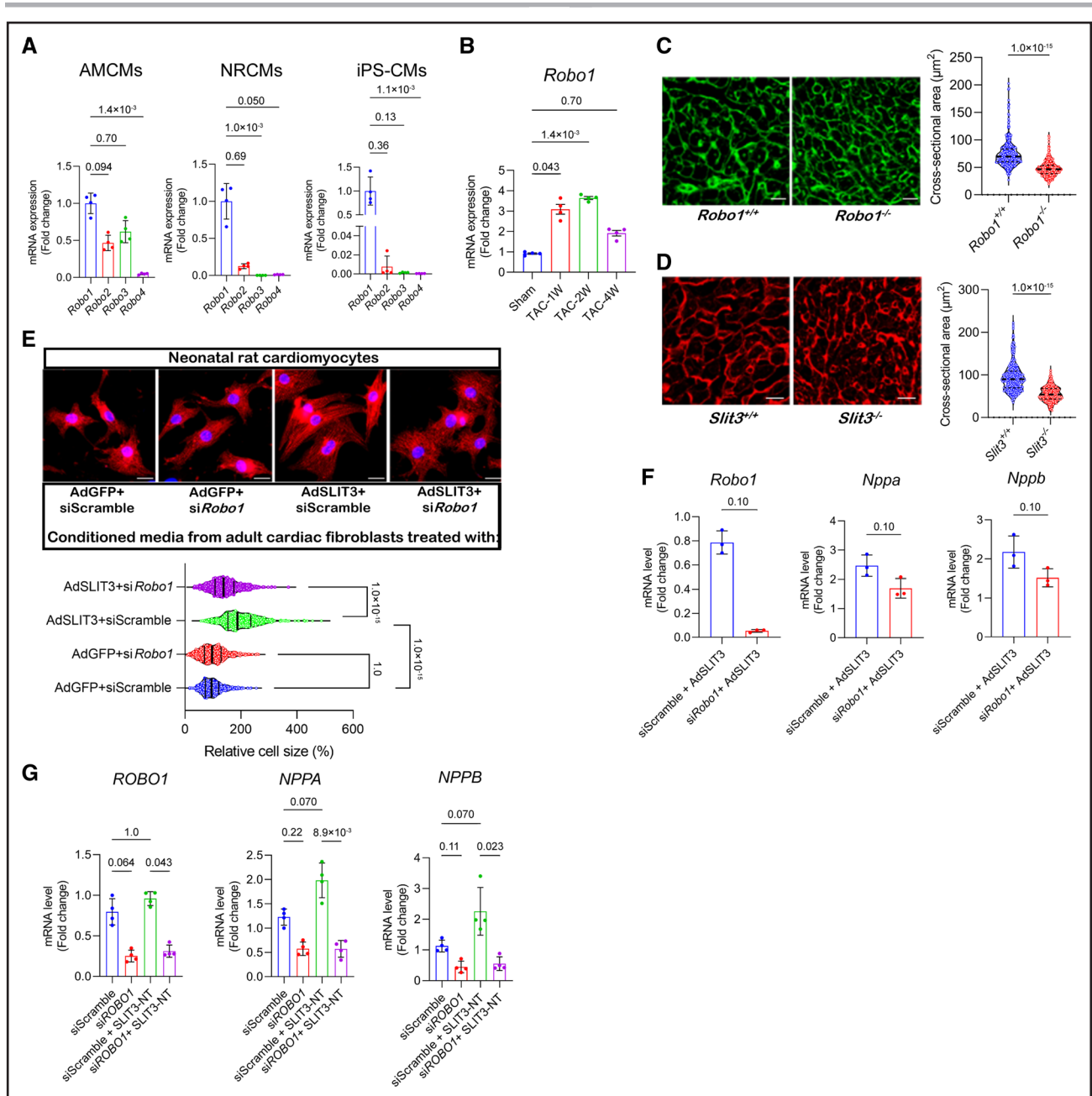
Figure 7. The in vitro hypertrophic effect of SLIT3 on cardiomyocytes is ROBO1-dependent.

A, Transcript levels of *Robo1*, *Robo2*, *Robo3*, and *Robo4* in cardiomyocytes of different origins. *Robo3* transcripts were not detectable in neonatal rat cardiomyocytes (NRCMs). N=3 independent experiments. **B**, Transcript levels of *Robo1* in mice heart tissue subjected to sham or transverse aortic constriction (TAC) surgery. N=4 mice/group. **C**, Representative images of wheat germ agglutinin (WGA)–stained heart sections and quantification of cardiomyocyte cross-sectional area from 7-d-old *Robo1* knockout mice (*Robo1^{-/-}*) or wild-type (WT) littermates (*Robo1^{+/+}*). Scale bar, 10 μm. N=400 cells from 3 mice/group. **D**, Representative images of WGA-stained heart sections and quantification of cardiomyocyte cross-sectional area from 7-d-old *Slit3^{-/-}* or WT littermates (*Slit3^{+/+}*). Scale bar, 10 μm. N=400 cells from 3 mice/group. **E**, Immunofluorescence with anti-α-actinin antibody and 4′,6-diamidino-2-phenylindole (DAPI) counterstain of NRCMs that were treated with conditioned media from WT adult cardiac fibroblasts transduced with *AdGFP* or *AdSLIT3* and transfected with either *siScramble* or *siRobo1*. Cell size quantification was performed by analyzing N=500 cells per group. **F**, Corresponding *Robo1*, *Nppa*, and *Nppb* transcript levels in NRCMs measured by quantitative PCR (qPCR) after treatment with conditioned media for 48 h. N=3 independent experiments. **G**, Human iPS-derived cardiomyocytes were transfected with *siScramble* or *siROBO1* for 48 h and then treated with recombinant *SLIT3-NT* for 8 d. Transcript levels of *ROBO1*, *NPPA*, and *NPPB* were assessed by qPCR. N=3 independent experiment. The Kruskal-Wallis test with the Dunn multiple comparisons test was used in (**A**, **B**, **E**, and **G**). The Mann-Whitney *U* test was used in (**C**, **D**, and **F**). AMCM indicates adult mouse cardiomyocyte; and iPS-CM, induced pluripotent stem cell–derived cardiomyocyte.
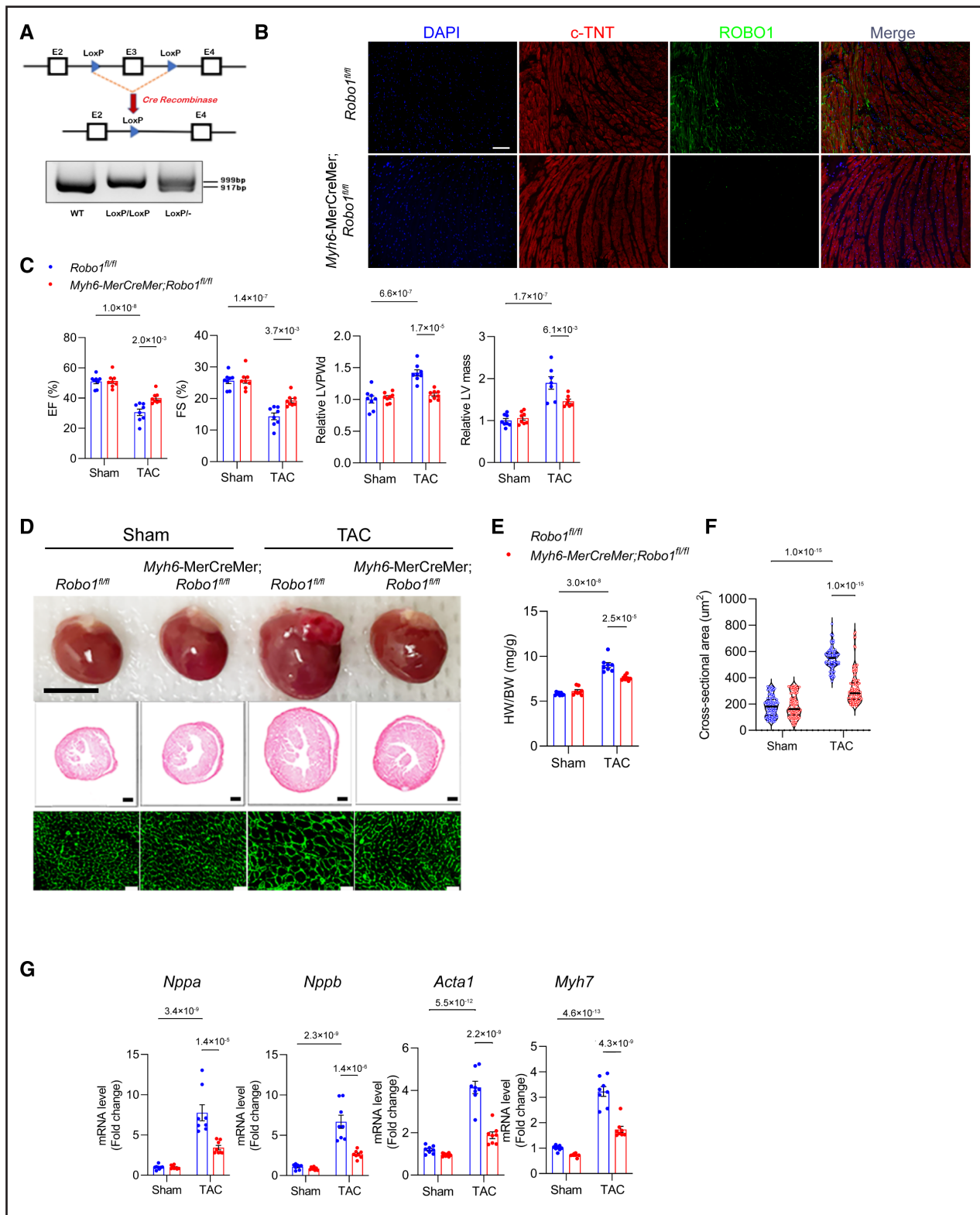
Figure 8. Cardiomyocyte-specific deletion of ROBO1 reduces cardiac hypertrophy and dysfunction after transverse aortic constriction (TAC).

A, Schematic of *Robo1^{fl/fl}* mouse model and PCR analysis for quantitation of *loxp*-flanked *Robo1* gene region in wild-type (WT), heterozygous (*loxp/-*), or homozygous (*loxp/loxp*) mice. **B**, Immunofluorescence staining using anti-cardiac troponin (c-TNT) antibody (red), anti-ROBO1 antibody (green), and 4',6-diamidino-2-phenylindole (DAPI; blue) of heart sections from *Robo1^{fl/fl}* control or *Myh6-CreERT2;Robo1^{fl/fl}* mice. **C**, B-mode and M-mode echocardiographies of Robo1^{fl/fl} or *Myh6-CreERT2;Robo1^{fl/fl}* mice after sham or TAC surgery with analysis of ejection fraction (EF), fractional shortening (FS), relative end-diastolic left ventricle posterior wall thickness (LVPWd), and relative left ventricle mass. N=8 mice/group. **D**, Explanted hearts from *Robo1^{fl/fl}* and *Myh6-MerCreMer;Robo1^{fl/fl}* mice after sham or TAC surgery (**top**); representative (*Continued*)

mice and confirming the stromal cell origin of the *SLIT3* ligand in the adult heart.

Factors expressed by CNMs are known to regulate cardiac function during healthy and disease states,[53–55] and our findings indicate that *SLIT3* is a critical cardiac stromal cell-derived paracrine factor that regulates the cardiomyocyte response to pressure overload. Our in vitro results reveal that *SLIT3* secreted by cardiac fibroblasts and vascular mural cells can directly stimulate cardiomyocyte hypertrophy, an effect that could be blunted by an anti-*SLIT3* neutralizing antibody. While cardiac fibroblasts are known to modulate the hypertrophic response,[56–58] the influence of vascular mural cells such as cardiac pericytes, a prevalent type of cardiac stromal cell,[59] on cardiac homeostasis and hypertrophy is poorly understood.[60] We provide the first evidence that vascular mural cells regulate the cardiomyocyte hypertrophic response to pressure overload via the secretion of *SLIT3*. This finding expands the known functional repertoire of cardiac vascular mural cells beyond that of vascular support[61] and control of vascular tone.[61,62]

The cardiovascular phenotype that resulted from SLIT3 deletion was dependent on the cellular sources that were targeted. Interestingly, global and stromal cell–specific deletion of SLIT3 inhibited pressure overload–induced cardiac hypertrophy to similar degrees. The absence of a linear and directly proportional effect on cardiac hypertrophy in the context of tissue-specific SLIT3 knockouts indicates a more complex relationship. Several alternative explanations could account for our findings. For instance, deleting SLIT3 in one cell type (eg, cardiac fibroblasts) might alter the biomechanical properties of the myocardium, thereby influencing *SLIT3* transcription in another cell population (eg, vascular mural cells). Conversely, removing SLIT3 in a different cell population (eg, vascular mural cells) could trigger the release of an unknown factor that then regulates *SLIT3* transcription in another cell population (eg, cardiac fibroblasts). Another possibility is that a threshold amount of SLIT3 is needed to regulate hypertrophy. This on/off response has been previously documented for *Myh6* and *Myh7* transcription in response to TAC.[63] Addressing these hypotheses necessitates further investigation into the factors governing *SLIT3* transcription in these specific cell types, a significant and intricate topic that extends well beyond the scope of our current study.

A more stoichiometric relationship was observed between SLIT3 and cardiac collagen. Only acute, global deletion of SLIT3 resulted in decreased fibrosis-related gene transcription under both basal and pressure overload conditions. Fibroblast-specific deletion of SLIT3 reduced *Col1a1* and *Col3a1* transcription induced by LV pressure overload, while vascular mural cell–specific deletion of SLIT3 only reduced *Col1a1* transcription after TAC. On the other hand, interfering with SLIT3 signaling by ROBO1 deletion in cardiomyocytes only reduced hypertrophy while not impacting cardiac fibrosis. Our results provide important insight into how SLIT3, a cardiac stromal cell-derived factor, can stimulate both components of adverse cardiac remodeling: cardiac fibrosis and cardiac hypertrophy.

Determining the cell-surface receptor for SLIT3 is necessary to understand how this secreted ligand imparts its hypertrophic effects on cardiomyocytes. Full-length SLIT proteins can be cleaved into 2 bioactive N- and C-terminal fragments.[64] SLIT fragments have different cell association characteristics in cell culture, suggesting that they may also have different extents of diffusion and binding properties and, hence, different functional activities in vivo.[64] ROBO-mediated signaling is initiated by the N-terminal fragment of SLIT ligands, while the C-terminal fragment of SLITs has been shown to bind PlexinA1.[30] Our initial results demonstrated that SLIT3-NT is responsible for the hypertrophic effects of SLIT3 on cardiomyocytes, suggesting the involvement of a roundabout receptor. We found that ROBO1 was predominantly expressed in cardiomyocytes compared with the other roundabout receptors, and the ROBO1 expression was stimulated in hearts after TAC, paralleling the induction of SLIT3 expression. Importantly, the deletion of ROBO1 in cardiomyocytes recapitulated the phenotypes exhibited in SLIT3 global, conditional, and tissue-specific knockout mice. Thus, we have provided several lines of evidence to indicate that ROBO1 mediates the regulatory effects of SLIT3 in cardiomyocytes. As such, the current study is the first to describe the role of SLIT3-ROBO1 signaling in postnatal cardiac function and disease. We did not observe any other clinical phenotypes in other organ systems at homeostasis or under pressure overload conditions although we did not perform a detailed microscopic or molecular investigation into other extracardiac tissues and organs in SLIT3 deficient mice.

In addition to those highlighted above, there are also other important, unanswered questions about the role of SLIT3-ROBO1 in postnatal cardiac function. Cardiac fibroblasts and vascular mural cells are heterogeneous populations of cells, and the subpopulations expressing SLIT3 have yet to be identified. The signaling pathways downstream of SLIT3-ROBO1 leading to

Figure 8 Continued. images of heart sections stained with hematoxylin & eosin (H&E; scale bar, 500 µm; **middle**); and representative images of wheat germ agglutinin (WGA)–stained heart sections (scale bar, 20 µm; **bottom**). **E**, Heart weight to body weight (HW/BW) ratio in *Robo1fl/fl* and *Myh6-MerCreMer* mice after sham or TAC surgery. N=8 mice/group. **F**, Quantification of myocyte cross-sectional area on WGA staining. **G**, Quantitative PCR (qPCR) analysis of transcription of hypertrophy-related genes (*Nppa*, *Nppb*, *Myh7*, and *Acta1*, normalized to *Gapdh* mRNA levels) in hearts from *Robo1fl/fl* or *Myh6-MerCreMer;Robo1fl/fl* mice after sham or TAC surgery. Two-way ANOVA and the Tukey multiple comparisons test were used for all comparisons.

the hypertrophic response in cardiomyocytes remain undefined. The importance of SLIT3 in regulating physiological hypertrophy of exercise or pregnancy is also unknown and will need a different animal model to evaluate this. The details of how SLIT3 modulates adult cardiac fibroblast function are also unknown and are currently under active investigation in our laboratory. Finally, the mechanisms by which pathological stimuli promote SLIT3 secretion from stromal cells and the roles of SLIT3 in other types of cardiovascular conditions, such as coronary artery and valvular heart disease, are unknown.

In conclusion, the secreted axon guidance molecule SLIT3 controls pressure overload–induced cardiac fibrosis and cardiomyocyte hypertrophy, with the latter via the ROBO1 receptor. These findings highlight SLIT3 as a novel mediator of pathological cardiac hypertrophy and fibrosis in the postnatal period, expanding the functional repertoire of this conserved glycoprotein ligand.

ARTICLE INFORMATION

Affiliations

Department of Cardiac Surgery (X.L., B.L., S.W., D.X., M.-S.S.) and Division of Cardiovascular Medicine, Department of Internal Medicine (A.M.D.R., T.H.), Michigan Medicine, Ann Arbor. Department of Cardiology, Shanghai Institute of Cardiovascular Diseases, Zhongshan Hospital, Shanghai Medical College of Fudan University, China (X.L., R.C.). Department of Pediatric Cardiology, Xinhua Hospital, School of Medicine, Shanghai Jiao Tong University, China (B.L.). Division of Cardiac Surgery, Department of Surgery (E.Z., M.S., M.-S.S.) and Department of Pediatrics (M.T.), David Geffen School of Medicine University of California, Los Angeles. Skaggs School of Pharmacy and Pharmaceutical Sciences (S.M.E.) and Department of Medicine, School of Medicine (S.M.E.), University of California, San Diego, La Jolla. Department of Internal Medicine, Cardiovascular Research Center, Yale University School of Medicine, New Haven, CT (A.E.). INSERM, Paris Cardiovascular Research Center (PARCC), Université de Paris, France (A.E.). Division of Biology and Medicine, Department of Neuroscience, Brown University, Providence, RI (A.J.). Life Sciences Institute, University of Michigan, Ann Arbor (S.W.).

Acknowledgments

Sources of Funding

Disclosures

None.

REFERENCES

1. Frangogiannis NG. The extracellular matrix in ischemic and nonischemic heart failure. *Circ Res*. 2019;125:117–146. doi: 10.1161/CIRCRESAHA.119.311148

2. de Boer RA, De Keulenaer G, Bauersachs J, Brutsaert D, Cleland JG, Diez J, Du XJ, Ford P, Heinzel FR, Lipson KE, et al. Towards better definition, quantification and treatment of fibrosis in heart failure. A scientific roadmap by the committee of translational research of the Heart Failure Association (HFA) of the European Society of Cardiology. *Eur J Heart Fail*. 2019;21:272–285. doi: 10.1002/ejhf.1406

3. Meagher P, Adam M, Civitarese R, Bugyei-Twum A, Connelly KA. Heart failure with preserved ejection fraction in diabetes: mechanisms and management. *Can J Cardiol*. 2018;34:632–643. doi: 10.1016/j.cjca.2018.02.026

4. Sharma K, Kass DA. Heart failure with preserved ejection fraction: mechanisms, clinical features, and therapies. *Circ Res*. 2014;115:79–96. doi: 10.1161/CIRCRESAHA.115.302922

5. Ytrehus K, Hulot JS, Perrino C, Schiattarella GG, Madonna R. Perivascular fibrosis and the microvasculature of the heart. Still hidden secrets of pathophysiology? *Vascul Pharmacol*. 2018;107:78–83. doi: 10.1016/j.vph.2018.04.007

6. Nakamura M, Sadoshima J. Mechanisms of physiological and pathological cardiac hypertrophy. *Nat Rev Cardiol*. 2018;15:387–407. doi: 10.1038/s41569-018-0007-y

7. Frangogiannis NG. Cardiac fibrosis. *Cardiovasc Res*. 2021;117:1450–1488. doi: 10.1093/cvr/cvaa324

8. Weeks KL, McMullen JR. The athlete's heart vs. the failing heart: can signaling explain the two distinct outcomes? *Physiology (Bethesda)*. 2011;26:97–105. doi: 10.1152/physiol.00043.2010

9. Wang H, Xie Y, Guan L, Elkin K, Xiao J. Targets identified from exercised heart: killing multiple birds with one stone. *NPJ Regen Med*. 2021;6:23. doi: 10.1038/s41536-021-00128-0

10. Li J, Umar S, Amjedi M, Iorga A, Sharma S, Nadadur RD, Regitz-Zagrosek V, Eghbali M. New frontiers in heart hypertrophy during pregnancy. *Am J Cardiovasc Dis*. 2012;2:192–207.

11. Oldfield CJ, Duhamel TA, Dhalla NS. Mechanisms for the transition from physiological to pathological cardiac hypertrophy. *Can J Physiol Pharmacol*. 2020;98:74–84. doi: 10.1139/cjpp-2019-0566

12. Bernardo BC, Weeks KL, Pretorius L, McMullen JR. Molecular distinction between physiological and pathological cardiac hypertrophy: experimental findings and therapeutic strategies. *Pharmacol Ther*. 2010;128:191–227. doi: 10.1016/j.pharmthera.2010.04.005

13. Diez J. Arterial hypertension in patients with heart failure. *Heart Fail Clin*. 2014;10:233–242. doi: 10.1016/j.hfc.2013.12.004

14. Frohlich ED, Gonzalez A, Diez J. Hypertensive left ventricular hypertrophy risk: beyond adaptive cardiomyocytic hypertrophy. *J Hypertens*. 2011;29:17–26. doi: 10.1097/HJH.0b013e328340d787

15. Levy D, Anderson KM, Savage DD, Balkus SA, Kannel WB, Castelli WP. Risk of ventricular arrhythmias in left ventricular hypertrophy: the Framingham Heart Study. *Am J Cardiol*. 1987;60:560–565. doi: 10.1016/0002-9149(87)90305-5

16. Ghali JK, Kadakia S, Cooper RS, Liao YL. Impact of left ventricular hypertrophy on ventricular arrhythmias in the absence of coronary artery disease. *J Am Coll Cardiol*. 1991;17:1277–1282. doi: 10.1016/s0735-1097(10)80135-4

17. Siegel D, Cheitlin MD, Black DM, Seeley D, Hearst N, Hulley SB. Risk of ventricular arrhythmias in hypertensive men with left ventricular hypertrophy. *Am J Cardiol*. 1990;65:742–747. doi: 10.1016/0002-9149(90)91381-f

18. Schiattarella GG, Hill JA. Inhibition of hypertrophy is a good therapeutic strategy in ventricular pressure overload. *Circulation*. 2015;131:1435–1447. doi: 10.1161/CIRCULATIONAHA.115.013894

19. Xie M, Burchfield JS, Hill JA. Pathological ventricular remodeling: therapies: part 2 of 2. *Circulation*. 2013;128:1021–1030. doi: 10.1161/CIRCULATIONAHA.113.001879

20. Bisping E, Wakula P, Poteser M, Heinzel FR. Targeting cardiac hypertrophy: toward a causal heart failure therapy. *J Cardiovasc Pharmacol*. 2014;64:293–305. doi: 10.1097/FJC.0000000000000126

21. Heidenreich PA, Albert NM, Allen LA, Bluemke DA, Butler J, Fonarow GC, Ikonomidis JS, Khavjou O, Konstam MA, Maddox TM, et al; American Heart Association Advocacy Coordinating Committee. Forecasting the impact of heart failure in the United States: a policy statement from the American Heart Association. *Circ Heart Fail*. 2013;6:606–619. doi: 10.1161/HHF.0b013e318291329a

22. Nguyen BY, Azam T, Wang X. Cellular signaling cross-talk between different cardiac cell populations: an insight into the role of exosomes in the heart diseases and therapy. *Am J Physiol Heart Circ Physiol*. 2021;320:H1213–H1234. doi: 10.1152/ajpheart.00718.2020

23. Tirziu D, Giordano FJ, Simons M. Cell communications in the heart. *Circulation*. 2010;122:928–937. doi: 10.1161/CIRCULATIONAHA.108.847731

24. Gong L, Wang S, Shen L, Liu C, Shenouda M, Li B, Liu X, Shaw JA, Wineman AL, Yang Y, et al. SLIT3 deficiency attenuates pressure overload-induced cardiac fibrosis and remodeling. *JCI Insight*. 2020;5:e136852. doi: 10.1172/jci.insight.136852

25. Kidd T, Bland KS, Goodman CS. Slit is the midline repellent for the robo receptor in Drosophila. *Cell*. 1999;96:785–794. doi: 10.1016/s0092-8674(00)80589-9

26. Blockus H, Chedotal A. Slit-Robo signaling. *Development*. 2016;143:3037–3044. doi: 10.1242/dev.132829

27. Mommersteeg MT, Yeh ML, Parnavelas JG, Andrews WD. Disrupted Slit-Robo signalling results in membranous ventricular septum defects and bicuspid aortic valves. *Cardiovasc Res*. 2015;106:55–66. doi: 10.1093/cvr/cvv040

28. Mommersteeg MT, Andrews WD, Ypsilanti AR, Zelina P, Yeh ML, Norden J, Kispert A, Chedotal A, Christoffels VM, Parnavelas JG. Slit-roundabout signaling regulates the development of the cardiac systemic venous return and pericardium. *Circ Res*. 2013;112:465–475. doi: 10.1161/CIRCRESAHA.112.277426

29. Liu J, Zhang L, Wang D, Shen H, Jiang M, Mei P, Hayden PS, Sedor JR, Hu H. Congenital diaphragmatic hernia, kidney agenesis and cardiac defects associated with Slit3-deficiency in mice. *Mech Dev*. 2003;120:1059–1070. doi: 10.1016/s0925-4773(03)00161-8

30. Delloye-Bourgeois C, Jacquier A, Charoy C, Reynaud F, Nawabi H, Thoinet K, Kindbeiter K, Yoshida Y, Zagar Y, Kong Y, et al. PlexinA1 is a new Slit receptor and mediates axon guidance function of Slit C-terminal fragments. *Nat Neurosci*. 2015;18:36–45. doi: 10.1038/nn.3893

31. Medioni C, Bertrand N, Mesbah K, Hudry B, Dupays L, Wolstein O, Washkowitz AJ, Papaioannou VE, Mohun TJ, Harvey RP, et al. Expression of Slit and Robo genes in the developing mouse heart. *Dev Dyn*. 2010;239:3303–3311. doi: 10.1002/dvdy.22449

32. Chowdhury UK, Jha A, Ray R, Kalaivani M, Hasija S, Kumari L, Chauhan A. Histopathology of the right ventricular outflow tract and the relation to hemodynamics in patients with repaired tetralogy of Fallot. *J Thorac Cardiovasc Surg*. 2019;158:1173–1183.e5. doi: 10.1016/j.jtcvs.2019.03.118

33. Hagdorn QAJ, Kurakula K, Koop AC, Bossers GPL, Mavrogiannis E, van Leusden T, van der Feen DE, de Boer RA, Goumans MTH, Berger RMF. Volume load-induced right ventricular failure in rats is not associated with myocardial fibrosis. *Front Physiol*. 2021;12:557514. doi: 10.3389/fphys.2021.557514

34. Ventura A, Kirsch DG, McLaughlin ME, Tuveson DA, Grimm J, Lintault L, Newman J, Reczek EE, Weissleder R, Jacks T. Restoration of p53 function leads to tumour regression in vivo. *Nature*. 2007;445:661–665. doi: 10.1038/nature05541

35. Kim BJ, Lee YS, Lee SY, Baek WY, Choi YJ, Moon SA, Lee SH, Kim JE, Chang EJ, Kim EY, et al. Osteoclast-secreted SLIT3 coordinates bone resorption and formation. *J Clin Invest*. 2018;128:1429–1441. doi: 10.1172/JCI91086

36. Ivey MJ, Kuwabara JT, Pai JT, Moore RE, Sun Z, Tallquist MD. Resident fibroblast expansion during cardiac growth and remodeling. *J Mol Cell Cardiol*. 2018;114:161–174. doi: 10.1016/j.yjmcc.2017.11.012

37. Kanisicak O, Khalil H, Ivey MJ, Karch J, Maliken BD, Correll RN, Brody MJ, Lin SCJ, Aronow BJ, Tallquist MD, et al. Genetic lineage tracing defines myofibroblast origin and function in the injured heart. *Nat Commun*. 2016;7:12260. doi: 10.1038/ncomms12260

38. Conway SJ, Molkentin JD. Periostin as a heterofunctional regulator of cardiac development and disease. *Curr Genomics*. 2008;9:548–555. doi: 10.2174/138920208786847917

39. Venugopal H, Hanna A, Humeres C, Frangogiannis NG. Properties and functions of fibroblasts and myofibroblasts in myocardial infarction. *Cells*. 2022;11:1386. doi: 10.3390/cells11091386

40. Kamo T, Akazawa H, Komuro I. Cardiac nonmyocytes in the hub of cardiac hypertrophy. *Circ Res*. 2015;117:89–98. doi: 10.1161/CIRCRESAHA.117.305349

41. Skelly DA, Squiers GT, McLellan MA, Bolisetty MT, Robson P, Rosenthal NA, Pinto AR. Single-cell transcriptional profiling reveals cellular diversity and intercommunication in the mouse heart. *Cell Rep*. 2018;22:600–610. doi: 10.1016/j.celrep.2017.12.072

42. Tallquist MD, Molkentin JD. Redefining the identity of cardiac fibroblasts. *Nat Rev Cardiol*. 2017;14:484–491. doi: 10.1038/nrcardio.2017.57

43. Crisan M, Yap S, Casteilla L, Chen CW, Corselli M, Park TS, Andriolo G, Sun B, Zheng B, Zhang L, et al. A perivascular origin for mesenchymal stem cells in multiple human organs. *Cell Stem Cell*. 2008;3:301–313. doi: 10.1016/j.stem.2008.07.003

44. Wang S, Huang S, Johnson S, Rosin V, Lee J, Colomb E, Witt R, Jaworski A, Weiss SJ, Si MS. Tissue-specific angiogenic and invasive properties of human neonatal thymus and bone MSCs: role of SLIT3-ROBO1. *Stem Cells Transl Med*. 2020;9:1102–1113. doi: 10.1002/sctm.19-0448

45. Guimaraes-Camboa N, Cattaneo P, Sun Y, Moore-Morris T, Gu Y, Dalton ND, Rockenstein E, Masliah E, Peterson KL, Stallcup WB, et al. Pericytes of multiple organs do not behave as mesenchymal stem cells in vivo. *Cell Stem Cell*. 2017;20:345–359.e5. doi: 10.1016/j.stem.2016.12.006

46. Foo SS, Turner CJ, Adams S, Compagni A, Aubyn D, Kogata N, Lindblom P, Shani M, Zicha D, Adams RH. Ephrin-B2 controls cell motility and adhesion during blood-vessel-wall assembly. *Cell*. 2006;124:161–173. doi: 10.1016/j.cell.2005.10.034

47. Ozerdem U, Grako KA, Dahlin-Huppe K, Monosov E, Stallcup WB. NG2 proteoglycan is expressed exclusively by mural cells during vascular morphogenesis. *Dev Dyn*. 2001;222:218–227. doi: 10.1002/dvdy.1200

48. Miano JM, Cserjesi P, Ligon KL, Periasamy M, Olson EN. Smooth muscle myosin heavy chain exclusively marks the smooth muscle lineage during mouse embryogenesis. *Circ Res*. 1994;75:803–812. doi: 10.1161/01.res.75.5.803

49. Patel K, Nash JA, Itoh A, Liu Z, Sundaresan V, Pini A. Slit proteins are not dominant chemorepellents for olfactory tract and spinal motor axons. *Development*. 2001;128:5031–5037. doi: 10.1242/dev.128.24.5031

50. Gara RK, Kumari S, Ganju A, Yallapu MM, Jaggi M, Chauhan SC. Slit/ROBO pathway: a promising therapeutic target for cancer. *Drug Discov Today*. 2015;20:156–164. doi: 10.1016/j.drudis.2014.09.008

51. Liu Z, Patel K, Schmidt H, Andrews W, Pini A, Sundaresan V. Extracellular Ig domains 1 and 2 of ROBO are important for ligand (Slit) binding. *Mol Cell Neurosci*. 2004;26:232–240. doi: 10.1016/j.mcn.2004.01.002

52. Chen JH, Wen L, Dupuis S, Wu JY, Rao Y. The N-terminal leucine-rich regions in Slit are sufficient to repel olfactory bulb axons and subventricular zone neurons. *J Neurosci*. 2001;21:1548–1556. doi: 10.1523/JNEUROSCI.21-05-01548.2001

53. Howard CM, Baudino TA. Dynamic cell-cell and cell-ECM interactions in the heart. *J Mol Cell Cardiol*. 2014;70:19–26. doi: 10.1016/j.yjmcc.2013.10.006

54. Davis J, Molkentin JD. Myofibroblasts: trust your heart and let fate decide. *J Mol Cell Cardiol*. 2014;70:9–18. doi: 10.1016/j.yjmcc.2013.10.019

55. Fountoulaki K, Dagres N, Iliodromitis EK. Cellular communications in the heart. *Card Fail Rev*. 2015;1:64–68. doi: 10.15420/cfr.2015.1.2.64

56. Xiang FL, Fang M, Yutzey KE. Loss of beta-catenin in resident cardiac fibroblasts attenuates fibrosis induced by pressure overload in mice. *Nat Commun*. 2017;8:712. doi: 10.1038/s41467-017-00840-w

57. Takeda N, Manabe I, Uchino Y, Eguchi K, Matsumoto S, Nishimura S, Shindo T, Sano M, Otsu K, Snider P, et al. Cardiac fibroblasts are essential for the adaptive response of the murine heart to pressure overload. *J Clin Invest*. 2010;120:254–265. doi: 10.1172/JCI40295

58. Moore-Morris T, Guimaraes-Camboa N, Banerjee I, Zambon AC, Kisseleva T, Velayoudon A, Stallcup WB, Gu Y, Dalton ND, Cedenilla M, et al. Resident fibroblast lineages mediate pressure overload-induced cardiac fibrosis. *J Clin Invest*. 2014;124:2921–2934. doi: 10.1172/JCI74783

59. Nees S, Weiss DR, Senftl A, Knott M, Forch S, Schnurr M, Weyrich P, Juchem G. Isolation, bulk cultivation, and characterization of coronary microvascular pericytes: the second most frequent myocardial cell type in vitro. *Am J Physiol Heart Circ Physiol*. 2012;302:H69–H84. doi: 10.1152/ajpheart.00359.2011

60. Alex L, Frangogiannis NG. Pericytes in the infarcted heart. *Vasc Biol*. 2019;1:H23–H31. doi: 10.1530/VB-19-0007

61. Sweeney M, Foldes G. It takes two: endothelial-perivascular cell cross-talk in vascular development and disease. *Front Cardiovasc Med*. 2018;5:154. doi: 10.3389/fcvm.2018.00154

62. O'Farrell FM, Mastitskaya S, Hammond-Haley M, Freitas F, Wah WR, Attwell D. Capillary pericytes mediate coronary no-reflow after myocardial ischaemia. *Elife*. 2017;6:e29280. doi: 10.7554/eLife.29280

63. Pandya K, Cowhig J, Brackhan J, Kim HS, Hagaman J, Rojas M, Carter CW Jr, Mao L, Rockman HA, Maeda N, et al. Discordant on/off switching of gene expression in myocytes during cardiac hypertrophy in vivo. *Proc Natl Acad Sci U S A*. 2008;105:13063–13068. doi: 10.1073/pnas.0805120105

64. Chedotal A. Slits and their receptors. *Adv Exp Med Biol*. 2007;621:65–80. doi: 10.1007/978-0-387-76715-4_5